Title

A zebrafish system for identifying genetic dependencies in melanocytes and melanoma

Authors

Sarah Perlee[1,2], Yilun Ma[1,3,4], Miranda V. Hunter[1], Jacob B. Swanson[5,6], Zhitao Ming[7], Julia Xia[1], Timothée Lionnet[5,6,8], Maura McGrail[7], Richard M. White[1,9, *]

Affiliations

[1]Department of Cancer Biology and Genetics, Memorial Sloan Kettering Cancer Center, New York, NY, USA

[2]Gerstner Sloan Kettering Graduate School of Biomedical Sciences, Memorial Sloan Kettering Cancer Center, New York, NY, USA.

[3]Weill Cornell/Rockefeller/Sloan Kettering Tri-Institutional MD-PhD Program, Memorial Sloan Kettering Cancer Center, New York, NY, USA.

[4]Cell and Developmental Biology Program, Weill Cornell Graduate School of Medical Sciences, New York, NY, USA.

[5]Institute for Systems Genetics, NYU Grossman School of Medicine, New York, NY, USA.

[6]Department of Cell Biology, NYU Grossman School of Medicine, New York, NY, USA.

[7]Department of Genetics, Development and Cell Biology, Iowa State University, IA, USA.

[8]Department of Biomedical Engineering, NYU Tandon School of Engineering, Brooklyn, NY.

[9]Nuffield Department of Medicine, Ludwig Institute for Cancer Research, University of Oxford, Oxford, UK.

[*] Corresponding Author: richard.white@ludwig.ox.ac.uk

ABSTRACT

The advent of large-scale sequencing in both development and disease has identified large numbers of candidate genes that may be linked to important phenotypes. Validating the function of these candidates *in vivo* is challenging, due to low efficiency and low throughput of most model systems. This is especially the case in skin cells such as melanocytes, where the background mutation rate is high. We have developed a rapid and scalable system for assessing the role of candidate genes in a melanocyte specific manner using zebrafish. We generated transgenic zebrafish in which Cas9 was knocked-in to the endogenous *mitfa* locus, a master transcription factor of the melanocyte lineage. By introducing single guide RNA expression cassettes into *mitfa*^{Cas9} embryos, we were able to achieve highly efficient melanocyte-specific mutation of genes important for melanocyte patterning and survival. These animals can be used to screen for dominant or recessive pigment defects in both the F0 generation (3 days) and F1 generation (3 months). We also utilized the *mitfa*^{Cas9} line to study the role of melanoma genetic dependencies such as SOX10, demonstrating that loss of SOX10 reduces melanoma initiation yet promotes tumor progression by a switch to a SOX9^{hi} state. This SOX10 to SOX9 switch has previously been observed in human patients, indicating that our system can be used to rapidly uncover biological states with relevance to human disease. Our high efficiency genetic approach can be readily applied to other cell lineages, with relevance to both development and disease.

INTRODUCTION

Zebrafish (*Danio rerio*) have emerged as a powerful model organism for studying various biological processes in melanocytes and melanoma cells. ENU based screens have enabled the identification of hundreds of germline alleles with seemingly tissue specific defects (*1-4*). More recently, CRISPR-based strategies, including the use of plasmid or ribonucleoprotein (RNP) delivery systems, have enabled generation of site-specific mutations in zebrafish with high precision and efficiency (*5-7*). Despite these advances, germline knockout makes it difficult to determine whether the identified gene has a specific function in a particular lineage, or whether the phenotype reflects a more general developmental defect. Furthermore, many genes which might have lineage specific functions cannot be studied using germline knockout, since embryonic lethality often accompanies global knockout of essential genes (*3*).

Pigmentation is one of the most well studied phenotypes in zebrafish. Mutations in several genes such as *sox10, ednrb, jam3b, puma, meox1* and *kit* yield clear defects in melanocyte/melanophore development, but these mutants also have defects in other tissues (*8-14*). Zebrafish have also been used to study melanoma, a pigmented tumor that arises from melanocytes or their neural crest precursors (*15-18*). These tumors are most commonly generated using whole-animal knockout of tumor suppressors such as *p53 (18).* The global loss of *p53* often results in a wide array of spontaneous tumors including angiosarcoma, leukemia, and MPNSTs, again confounding our ability to understand melanocyte-specific genes in the context of melanoma (*19*).

Efficient cell type-specific knockout of genes is crucial for unraveling the intricate molecular mechanisms underlying melanocyte function, development, and transformation. To overcome the limitations of global knockout methods, several groups have explored several tissue-specific and

conditional knockout strategies in zebrafish (*20-27*). For example, the MAZERATI system uses tissue-specific promoter transgenes to drive Cas9 expression, which are introduced via plasmid injection into one-cell stage embryos with Tol2 transposase to enable genomic integration (*21, 28*). Despite these advancements, efficiency remains of paramount importance. In normal development, low-efficiency knockout of a gene can mask important phenotypes, as the mutant cells can readily be outcompeted by wild-type or inframe mutations. Efficiency is even more important in the cancer context. Mutation of a tumor suppressor (i.e., PTEN) need not be highly efficient, since clones with a Darwinian advantage will inevitably outcompete other clones. However, in situations where we want to study necessity of a tumor promoting gene in vivo (i.e., an oncogene), cells which have mutations of a key driver gene will easily be outcompeted by nearby clones. Such efficiency is critical as sequencing projects such as All of Us, the UK Biobank and the Cancer DepMap continue to identify hundreds of new candidate genes on a regular basis (*29-31*), many of which have yet to be characterized *in vivo*.

In this study, we wished to build upon this prior work to improve efficiency and scalability in the context of melanocytes and melanoma. Specific problems we wished to solve include the ability to work with wild-type strains with normal skin architecture (i.e., obviate the need for germline BRAF/p53/*mitfa* lines), the need for overexpression of *mitfa* rescue cassettes such as MiniCoopR (in which tumors become addicted to *mitfa*), and avoidance of large plasmids (which greatly reduce efficiency). Furthermore, we wished to avoid use of *mitfa* promoter fragments to drive Cas9, which lack many endogenous regulatory elements, and rely upon random Tol2-mediated integration (*32*). Depending on the location of integration, Cas9 may be expressed in unintended cell types and variability in number of integration events can lead to heterogenous levels of Cas9 expression in different cells.

To address these needs, we developed a lineage-specific Cas9 knock-in zebrafish model to efficiently investigate genetic dependencies in melanocytes and melanoma. By integrating the Cas9 nuclease into the endogenous melanocyte-specific *mitfa* locus, we achieved highly efficient and specific gene disruption across the melanocyte developmental lineage. We used our *mitfa*^{Cas9} knockin animals to inactivate the pigmentation gene *albino* and the embryonic essential genes *sox10* and *ptena/b* in melanocytes without additional developmental or off-target phenotypes. We also demonstrated that this system can be used to efficiently induce melanomas in wild-type fish by inactivating the tumor suppressors *p53* and *ptena/b* within melanocytes also expressing the melanoma oncogene BRAF^{V600E}. Inactivating the neural crest transcription factor *sox10* in these tumors significantly decreased melanoma initiation but resulted in rare invasive tumors that highly expressed the *sox9* transcription factor, similar to what has been described in vitro and thus validating that this phenomenon occurs *in vivo* (*33, 34*). Our system can thus be used to advance our understanding of melanocyte biology and the genetic underpinnings of phenotypic switching in melanoma.

RESULTS

Targeted integration of Cas9 to the *mitfa* locus

To selectively disrupt genes in a melanocyte lineage-specific manner, we established a transgenic zebrafish line harboring Cas9 at the endogenous *mitfa* locus. *Mitfa* expression is

detectable by 18 hours postfertilization (hpf) and is highly expressed in pigment cells including melanocytes, xanthophores and their progenitors. To achieve knock-in, we utilized the GeneWeld method, which enables efficient integration of DNA cassettes using homology mediated end joining (HMEJ) (*35, 36*). The knock-in cassette, containing Cas9 and BFP driven by the eye-specific γ-crystallin promoter, was targeted to exon 2 of the *mitfa* gene, which leads to disruption of the endogenous *mitfa* gene (Fig. 1A). We strategically selected this genomic site for several reasons. First, this is the sole exon shared among the three *mitfa* protein-coding transcripts. Furthermore, targeting Cas9 to exon 2 offers the flexibility of replicating this knock-in strategy in *casper* zebrafish, a transparent fish widely used for melanoma studies that harbor a premature stop codon in *mitfa* exon 3 (*37*).

The knock-in vector, along with Cas9 protein and guide RNAs targeting either the *mitfa* integration site or the sequences flanking the 5' and 3' homology arms, were injected into 1-cell stage wild-type Tropical 5D (T5D) zebrafish embryos (Figure 1B) (*38*). Embryos were raised to adulthood then crossed with WT T5D fish. The resulting F1 embryos were screened for BFP+ eyes, indicating successful integration, and tail clippings were sequenced to confirm precise integration of the knock-in cassette at the *mitfa* locus. We sequenced four F1 fish and detected on-target integration at the *mitfa* locus in all four fish (Figure S1A). In zebrafish, one copy of *mitfa* is sufficient for the normal development of neural crest-derived melanocytes, but loss of both copies of *mitfa* results in loss of the melanocyte lineage (*37, 39*). To determine the effect of a single copy of *mitfa*^{Cas9} on melanocytes, *mitfa*^{Cas9} fish were in-crossed and the resulting siblings were imaged at various time points (Fig. S1B). WT and *mitfa*^{Cas9} fish exhibited indistinguishable melanocyte patterning during both embryonic and adult stages. However, as expected, fish carrying two copies of Cas9 (*mitfa*$^{Cas9/Cas9}$) resembled the *nacre* mutant (*mitfa*-/-), characterized by complete loss of melanocytes and melanoblasts, indicating the endogenous *mitfa* gene is disrupted on knock-in alleles (*39*). We used zebrafish harboring one knock-in allele (*mitfa*^{Cas9}) for all subsequent experiments to allow us to test gene function in melanocytes.

To assess whether Cas9 expression was restricted to melanocytes, we performed fluorescence in situ hybridization (FISH) on 3 day postfertilization (dpf) WT and *mitfa*^{Cas9} embryos to measure *mitfa* and Cas9 mRNA expression (Figure 1C and S1C). Embryos were treated with 1-phenyl-2-thiourea (PTU) to block pigmentation and enable fluorescence imaging of melanocytes. In both WT and *mitfa*^{Cas9} fish, *mitfa* was detected within the embryonic melanocyte stripe regions as expected. In *mitfa*^{Cas9} fish, Cas9 mRNA was detected only within melanocyte stripe regions also expressing *mitfa*. These results provide functional validation for on-target integration and tissue-restricted expression of Cas9 to the melanocyte lineage.

Highly efficient knockout of *slc45a2/albino* in *mitfa*^{Cas9} fish

To assess the effectiveness of our stable *mitfa*^{Cas9} line, we first targeted the *albino* gene (*slc45a2*). This gene is one of the most well-known determinants of skin color variation in humans, and germline disruption has been well described in zebrafish and leads to a complete loss of pigmentation in melanocytes without disrupting melanocyte development (*40-42*). This distinct phenotype enables the visual observation of Cas9 activity in zebrafish injected with *albino* gRNA. To test our system, we designed plasmids, denoted MG-gRNA, containing a zU6:gRNA cassette followed by *mitfa*:GFP to enable visualization of cells expressing the *albino* gRNA. MG-*albino* and MG-NT were injected into one-cell stage embryos from crosses between

mitfa^{Cas9} and WT fish, which express Cas9 in all melanocytes but exhibit mosaic gRNA expression (Figure 2A).

Embryos were screened for BFP+ eyes to identify those harboring *mitfa*^{Cas9}. Upon adulthood, 92% of F0 MG-*albino* fish had mosaic loss of pigmentation within the melanocyte stripe regions (Figure 2B and C). Unpigmented regions maintained expression of mitfa-GFP (Fig. 2B), indicating that the breaks in melanocyte stripes arise from loss of pigmentation in melanocytes rather than loss of the melanocyte lineage (Figure 2B). As expected, control MG-NT clutch mates displayed normal pigmentation and GFP+ melanocytes were indistinguishable from GFP- regions on the same fish (Figure 2B and C).

We next aimed to determine the efficiency of *mitfa*^{Cas9} in the F1 generation, in which every melanocyte stably expresses the *albino* gRNA and *mitfa*^{Cas9}. To generate F1 lines, we outcrossed the F0 MG-gRNA fish to WT and sorted embryos for BFP+ eyes and GFP+ melanocytes. F1 MG-*albino* fish exhibited a near complete loss of pigmentation, demonstrating that our mitfa-Cas9 system is highly efficient in F1 fish (Figure 2D and E). To study the effect of *albino* inactivation across various stages of development, F1 MG-gRNA fish were once again outcrossed to WT, generating F2 MG-gRNA fish expressing one copy of mitfa-Cas9. Imaging revealed a measurable pigmentation loss in F2 MG-*albino* melanocytes as early as 3 days post-fertilization (dpf) (Fig. 2F and G). F2 MG-*albino* fish maintained loss of pigmentation throughout development, indicating the sustained activity of *mitfa*^{Cas9} (Fig. 2H to K).

To confirm on-target cutting of the *albino* gene just in the melanocyte lineage (and not other tissues), the skin from F1 MG-*albino* fish was dissected and GFP+ and GFP- cells were isolated using FACS (Fig. 2L). GFP+ cells should encompass *mitfa*-expressing melanocytes, xanthophores, and their progenitors, while GFP- cells represent other non-melanocytic, non-*mitfa* expressing skin cells, such as keratinocytes, fibroblasts, and immune cells. We performed CRISPR-seq on DNA from both populations to directly measure Cas9 efficiency and specificity, quantifying the proportion of indels at the *albino* locus. Although we have previously shown that FACS sorting melanocytic cells is possible, it is important to note that we often observe high levels of contaminating keratinocytes in FACS sorted melanocyte populations, which may lead to an underestimation of the true allelic frequency in our CRISPR-seq (*43*). Despite this, robust inactivation of the *albino* gene was observed in GFP+ (*mitfa*-expressing) cells, confirming somatic inactivation (Fig. 2M). The majority of indels were frame-shift inducing mutations. A likely PCR or sequencing artifact resulting in a “T” insertion was excluded from the frameshift indel percentage as it was observed in all conditions including WT fish with no pigmentation phenotype (Fig. S2A). These results confirm that our *mitfa*^{Cas9} system allows us to inactivate genes within the melanocytic lineage *in vivo* in a highly efficient and specific manner.

sox10 **is required for normal pigment cell patterning of adult zebrafish**

Having confirmed that our *mitfa*^{Cas9} system allows us to rapidly, efficiently and specifically manipulate melanocyte gene expression, we next wanted to target embryonic essential genes. Detecting “negative” gene knockout phenotypes such cell death can be challenging *in vivo* due to the selective advantage that WT cells have over mutants. It is possible to distinguish such phenotypes with germline knockout, but current tissue specific knockout systems lack the sensitivity to detect negative phenotypes. To assess the effectiveness of our *mitfa*^{Cas9} model in

detecting negative phenotypes, we utilized it to target *sox10*, a transcription factor vital to the neural crest lineage and indispensable for the survival of both zebrafish and mice (*8, 44*). Germline knockout of *sox10* in zebrafish leads to severe defects in peripheral nerve development and the complete absence of melanocytes (*8, 45, 46*). Consequently, a global knockout approach is not feasible for studying the function of *sox10* in adult melanocytes *in vivo*.

We leveraged our *mitfa*^{Cas9} system to specifically inactivate *sox10* in the melanocyte lineage. *mitfa*^{Cas9} fish injected with a MG-*sox10* plasmid exhibited noticeable gaps in their melanocyte stripes (Fig. 3A-B, S3A). Germline deletion of a *sox10* enhancer region similarly affects adult stripe patterning in zebrafish (*47*). In contrast to the *albino* F0 fish, the gaps in the stripes of the *sox10* F0 fish were not occupied by unpigmented GFP+ melanocytes, indicating a potential defect in the survival or differentiation of melanocytes upon loss of *sox10*. This phenotype became even more pronounced in the stable F1 lines, where several gaps are visible (Fig. 3C). Zebrafish have four dark stripes occupied by melanocytes, which alternate with light colored interstripes occupied by yellow pigmented xanthophores (*48*). Typically, melanocyte stripe 1D (dorsal) is wider than the interstripe X0 directly below it, as observed in MG-NT F1 fish (Fig. 3C and D, S3A). However, the opposite is true for MG-*sox10* F1 fish, where we observed an apparent widening of the interstripe region and narrowing of the melanocyte stripes (Fig. 3C and D, S3A). Melanocytes were counted in fish treated with epinephrine to aggregate melanosomes, revealing a significant reduction in the number of melanocytes in the F1 *sox10* KO fish compared to F1 NT fish (Fig. 3E). Reduction in GFP+ cells within the xanthophore interstripes (X0) suggested that *sox10* deficiency also negatively affected xanthophore populations, in line with previous work indicating a role for *sox10* in specifying both xanthophores and melanocytes in zebrafish embryos (*49*). This study is the first to demonstrate this phenomenon in adult fish. Besides the effects on pigment cells, MG-*sox10* F0 and F1 fish appeared otherwise healthy with no obvious abnormalities. These results demonstrate that our *mitfa*^{Cas9} knockout system can be used to study the roles of embryonic essential genes in melanocytes.

Targeting tumor suppressors with *mitfa*^{Cas9} induces melanoma

We next turned our attention to melanoma. In humans, tumor suppressors such as *PTEN* and *p53* are somatically inactivated in melanoma (*50, 51*). In contrast, the most commonly used zebrafish models of melanoma use a germline *p53* mutation, which is not typically seen in humans with the disease and precludes our ability to discern the role of *p53* inactivation specifically in melanocytes and melanoma (*18*). While global *p53* loss is not lethal, it does lead to a wide range of non-melanoma tumors, which can deteriorate fish health and confound melanoma studies (*19*). Furthermore, current zebrafish melanoma models typically involve the utilization of MiniCoopR *mitfa* rescue cassettes into *Casper* or *nacre* zebrafish, which are void of normal pigment cells. Although this method is highly efficient, it does not accurately represent melanoma initiation in the context of normal skin architecture and relies on artificial overexpression of *mitfa*. To mimic human melanoma initiation more accurately, we decided to use our *mitfa*^{Cas9} model to assess tumor initiation using melanoma-specific gene knockout in the context of a wild-type skin background. Previous studies have shown that expression of BRAF^{V600E} and loss of *p53* in WT (non-*Casper*) fish results in relatively low tumor burden, so we decided to also target *ptena* and *ptenb*, the zebrafish orthologs of human *PTEN* (*15*). *Ptena/ptenb* loss in combination with *p53* has been shown to accelerate melanoma formation in zebrafish (*52, 53*).

To first address the effect of *ptena/b* loss on normal melanocytes, we generated melanocyte-specific knockouts of *ptena* and *ptenb* (Fig. 4A). Like *sox10*, germline knockout of *ptena/b* is embryonic lethal (*54, 55*). In our *ptena/ptenb* F0 melanocyte-specific KO fish, we observed an expansion of the melanocytes outside of the stripe regions they normally are restrained to, suggesting that inactivation of *ptena* and *ptenb* induces defects in melanocyte patterning (Fig. 4A and B). However, loss of *ptena/b* alone was not sufficient to induce melanoma.

To generate tumors, we co-injected *mitfa*^{Cas9} embryos with plasmids encoding *mitfa:*BRAF^{V600E} and sgRNAs targeting *tp53* and *ptena*/*b* (Fig. 4C). Larvae were sorted for BFP+ eyes, indicating mitfa-Cas9 integration, and monitored for tumors over 30 weeks. No tumors were detected in BFP- fish from any of the injection conditions (n=136). We also did not observe any tumors in BFP+ fish injected with either BRAF^{V600E} alone (n=35) or ptena/b; p53 guides in the absence of BRAF^{V600E} (n=17). In contrast, tumors developed in all BFP+ groups injected with both *mitfa:*BRAF^{V600E} and gRNA plasmids. Approximately 5% of fish from the BRAF;*tp53* group developed tumors (Fig. 4D). This aligns with a previous study where 6% of *p53*-/- fish developed tumors when injected with a BRAF^{V600E} construct (*15*). Targeting of *ptena* and *ptenb* in *mitfa*^{Cas9} fish co-injected with *mitfa*:BRAF^{V600E} resulted in a higher tumor incidence of 29% (Fig. 4D).

When all three tumor suppressors (*p53, ptena, ptenb*) were targeted in combination with BRAF^{V600E}, 59% of fish developed tumors by 30 weeks post fertilization (wpf) (Fig. 4D). Immunohistochemistry (IHC) revealed that all tumor samples expressed BRAF^{V600E}, while p-AKT, a hallmark of *PTEN* inactivation, was only detected in samples with *ptena/b* KO (Fig. 4E). To confirm on-target cutting, DNA was extracted from tumors and CRISPR sequencing was performed on PCR amplicons for each tumor suppressor gene. A large proportion of reads contained indels at the target locus for each of the target genes (*ptena*, *ptenb*, and *p53*) (Fig. 4F and S4). Some tumors had an array of mutations, while others appeared to be composed largely of a one dominant clone (Fig. S4A to C). Our system thus allows us to rapidly dissect the melanocyte-specific function of both oncogenes (BRAF^{V600E}), as well as putative tumor suppressors (*p53, ptena/b*), while avoiding pleiotropic effects of global tumor suppressor loss.

Loss of *sox10* promotes melanoma phenotype switching *in vivo*

Our next objective was to leverage the mitfa^{Cas9} fish as a tool for identifying or validating potential genetic dependencies within melanoma. Genetic dependencies can be difficult to study *in vivo* since inactivation of a required gene inevitably leads to selection for non-mutant alleles, as has been previously shown (*17*). In melanoma, the DepMap identified *SOX10* as the top *in vitro* genetic dependency necessary for tumor cell proliferation (*31, 56*). *SOX10* is highly upregulated in melanoma tumors and is often used as a marker for malignant melanoma (*33*). Using our system, we aimed to discern the effect of *sox10* knockout on melanoma initiation. To assess this, we generated plasmids containing multiple sgRNAs driven by three distinct zU6 promoters (zU6A, zU6B, and zU6C) to simultaneously target both tumor suppressors (*p53, ptena/ptenb*) and tumor promoting genes (*sox10*) in the same cells, which reduces the chance of selecting for non-mutant alleles (*20*). We co-injected these plasmids with *mitfa*:BRAF^{V600E}, sorted fish for BFP+ eyes, and tracked tumor free survival over the course of 40 weeks (Fig. 5A and B). Consistent with the DepMap prediction, *sox10* inactivation markedly reduced tumor incidence, with only 3/96 (3.1%) fish with *sox10* knockout developing melanoma tumors

compared to the 20/94 fish (21.3%) from the NT condition that developed tumors (Fig. 5B). Using IHC, we validated that *sox10* KO tumors expressed lower levels of Sox10 protein compared to NT tumors (Fig. 5C and S5A). Quantification of Sox10 intensity with immunofluorescence confirmed this finding (Fig. S5B).

Although *sox10* clearly reduced tumor initiation, we noted that the few "escapers" which did generate tumors in this context appeared morphologically very distinct compared to the *sox10* intact tumors. Specifically, these tumors were highly invasive with a mesenchymal morphology compared to the typical $BRAF^{V600E}$ melanoma (Fig. 5C). This observation raised the possibility that these tumors had undergone "phenotype switching", a form of cell plasticity in which cells transition between proliferative and invasive states (*33, 34, 56, 57*). In melanoma, the proliferative state is thought to be characterized by high expression of *SOX10*, whereas the mesenchymal, invasive state is characterized by high expression of *SOX9* (*34*). These two highly related transcription factors have seemingly opposite and possibly antagonistic roles in melanoma. In prior work in both zebrafish and mice, loss of *sox10* is clearly associated with a loss of tumor initiating potential and cell proliferation (*17, 56*). In vitro, knockout of *SOX10* in a variety of human cell lines is associated with acquisition of a $SOX9^{hi}$ state, which has been suggested to be linked to the invasive phenotype (*34*). Re-analysis of publicly available RNA-seq data using 3 patient-derived human melanoma cell lines treated with siRNA targeting *SOX10* confirmed this observation, with the *SOX10* lines now becoming $SOX9^{hi}$ (Fig. 5E to J, S5C to L) (*34*). These data raised the hypothesis that the more invasive tumors we see in our escaper fish was due to gain of *sox9* expression. To test this, we stained our *sox10* CRISPR tumors for *sox9* and discovered that 2 of the 3 *sox10* KO tumors markedly upregulated *sox9* relative to control tumors expressing NT gRNA (Fig. 5C and D). This highlights the $mitfa^{Cas9}$ system as a potentially invaluable tool for validating *in vitro* discoveries.

Discussion

The ability to model genetic dependencies *in vivo* is one of the most important uses of model organisms. Forward genetic mutagenesis screens using compounds such as ENU or EMS led to the identification of many key developmental genes in organisms such as Drosophila, C. elegans, Saccharomyces, zebrafish, and many others (*1, 58*). These approaches have rapidly accelerated in the era of TALENs and CRISPR, readily allowing for knockout of nearly any gene in a wide variety of non-model organisms. Cre/Lox approaches have further augmented our ability to discern the cell-type specific effects of these genes, although these are still laborious and time consuming, especially in models such as mice.

Alongside these approaches have been remarkable advances in large scale sequencing of human tissues. GWAS-like efforts such as the UK Biobank and the US All of Us programs have identified thousands of germline variants (SNPs) that may be linked to interesting phenotype variation (*29, 30*). A conceptually similar approach is also happening in diseases such as cancer, in which efforts such as the TCGA, ICGC and DepMap have continued to unveil new potential somatic variants (SNVs) linked to cancer (*31, 59, 60*).

Across these efforts, in both development and disease, the large number of candidate variants makes it challenging to connect these genotypes to phenotypes. This is especially acute in melanoma, where the large number of somatic variants generated by UV radiation leads to a high number of background mutations that may or may not have pathogenic function. Thus, there is a

substantial need for *in vivo* models that allow for rapid and efficient modeling of candidate genes. Our development of the *mitfa*-Cas9 knockin line provides such a method. One major advantage is that phenotypes can be readily screened either in the F0 generation (as mosaics) or in the F1 generation (3 months later). The F1 fish in particular are advantageous, since they allow for highly efficient biallelic knockout of the gene of interest, allowing for very quick identification of genes that only have recessive phenotypes (i.e., *albino*). On a per gene basis, this saves well over 3 months of work compared to germline knockouts and uses vastly fewer animals since all F1 animals (even those for recessive alleles) are informative. Additionally, this model eliminates the issue of inbreeding, promoting healthier genetic lines and facilitating the potential for outcrossing with any available fish line. Because we demonstrate that the Cas9 is completely restricted to the melanocyte lineage, with no detectable off-target expression, this easily allows us to discern the melanocyte-specific effect of pleiotropic genes very efficiently.

One interesting observation of our melanoma studies is evidence that loss of melanoma genetic dependencies like *SOX10* (as suggested by the human DepMap data) can still lead to tumors, albeit with very different biological behaviors. In both the fish and in the human samples we analyzed, loss of *SOX10* leads to acquisition of a *SOX9*^{hi} state instead (*34*). *SOX9* is increasingly recognized to be a potent mediator of tumor cell invasiveness, which is what we observe in our fish (*61, 62*). One implication of this finding is that clinical targeting of transcription factors like *SOX10*, long considered an ideal therapeutic approach, could lead to unexpected outcomes in which tumors might proliferate less but become more invasive or resistant to therapy. Whether this phenomenon of *SOX10/SOX9* switching is a general phenomenon, or specific to that class of TFs, remains to be determined. However, a similar phenomenon has been observed for *MITF*, another melanocytic TF, suggesting this idea of TF switching needs to be more thoroughly explored in the future (*57, 63, 64*).

Our approach has several limitations, which will need to be addressed in future studies. Due to the constitutive nature of the Cas9, we have little control over the timing of its expression. Because it is knocked into the endogenous *mitfa* locus, the expression of Cas9 will vary with the endogenous regulation of that gene. In future iterations of this general approach, swapping the Cas9 for an inducible version would allow for better timed knockout of genes (*65*). Because *mitfa* itself is expressed in melanoblasts, melanophores and xanthophores during different stages of development, choosing a promoter (e.g. PMEL) that is more tightly restricted to melanocytes may be advantageous. Finally, although our system was relatively efficient, we still did not see 100% knockout. This may reflect that it is relatively easy to bypass the CRISPR lesion in an exon with an in-frame mutation. The use of multiple sgRNAs, or sgRNAs that target promoter regions, rather than exons, could further augment efficiency of knockout. Alternatively, instead of targeting DNA, we could consider using RNA targeting CRISPR enzymes. Recent work has shown that RNA degradation induced by Cas13 works in zebrafish and may allow for more nuanced knockdown rather than knockout of a given candidate gene (*66, 67*). This may especially have advantages in the context of melanoma, where genes are commonly dysregulated rather than completely knocked out. We envision it would be relatively straightforward to knock Cas13 into the locus of interest using an analogous approach to the one we have taken here.

Finally, while our studies clearly focused on the melanocyte lineage, highly similar approaches could be taken for virtually any cellular lineage in which master regulators or markers are

known. Given the large number of already identified promoter/enhancer fragments in the zebrafish, this would be an important extension of our system to study gene variants in the context of development and other diseases (*68*).

MATERIALS AND METHODS

Zebrafish husbandry and ethics statement

All zebrafish experiments adhered to institutional animal protocols and were conducted in compliance with approved procedures. Fish stocks were maintained at a temperature of 28.5 °C, under 14:10 light:dark cycles, with pH set at 7.4, and salinity-controlled conditions. The zebrafish were fed a standard diet comprising brine shrimp followed by Zeigler pellets. Approval for the animal protocols outlined in this manuscript was obtained from the Memorial Sloan Kettering Cancer Center (MSKCC) Institutional Animal Care and Use Committee (IACUC), under protocol number 12-05-008. Anesthesia was conducted using Tricaine (4 g/l, Syndel, Ferndale, WA, USA) from a stock of 4 g/l and diluted to 0.16 mg/ml. Adult zebrafish of both sexes were equally employed in all experiments. Embryos, collected through natural mating, were incubated in E3 buffer (5 mM NaCl, 0.17 mM KCl, 0.33 mM CaCl2, 0.33 mM MgSO4) at 28.5 °C. The wild-type strain used was Tropical 5D Zebrafish (T5D) (*38*).

GeneWeld plasmid construction

A combination of restriction enzyme digestion and HiFi cloning was used to construct the GeneWeld pPRISM-nCas9n, γcry1:BFP vector for targeted integration to isolate an nls-Cas9-nls knockin. A 765 bp fragment containing the Porcine teschovirus-1 polyprotein 2A peptide sequence was amplified from the pPRISM-2A-Cre, γcry1:BFP vector (Addgene #117789) with primers Ori-F and 2A-R (*35, 36*). The nCas9n cDNA was amplified from the expression vector pT3TS-nCas9n (Addgene #46757) with primers Cas9-F and Cas9-R (*69*). A KpnI/SpeI fragment containing the pPRISM-2A-Cre, gcry1:BFP vector backbone was assembled with the 2A and nCas9n PCR amplicons using the NEBuilder HiFi DNA Assembly Cloning Kit (NEB # E5520S) following the manufacturer's instructions.

Homology arms were designed as previously described (*35, 36*). Briefly, 48bp homology arms complementary to the *mitfa* target site were designed using GTagHD (http://www.genesculpt.org/gtaghd/) for the pPRISM GeneWeld plasmid series. The two pairs of complementary oligos can be found in Supplementary table 1. 5' and 3' arms were cloned sequentially into the pPRISM-nCas9n, γcry1:BFP vector. The 3' homology arm oligos were annealed and cloned into the vector using the BspQI restriction site as previously described. Due to the multiple BfuAI sites within Cas9, instead of using BfuAI restriction cloning, we alternatively used in-fusion cloning (Takara Bio) to insert a gBlock (IDT) containing the 5' homology arm into the pPRISM-nCas9n, gcry1:BFP vector. Primers and gblock sequence used for cloning are listed in Supplementary table 1. The 5' and 3' homology arms were sequenced with primers 5'homologycheckF and R3'_pgtag_seq, respectively.

Injection of GeneWeld reagents

Injections of GeneWeld reagents were performed on one-cell stage embryos. We used the Alt-R CRISPR-Cas9 system (IDT) for the initial knock-in of nCas9n, γcry1:BFP to the *mitfa* locus. In brief, 100 µM tracrRNA (IDT 1075928) was mixed at a 1:1 ratio with either *mitfa* crRNA or universal crRNA then incubated at 95 °C for 5 min. Recombinant Cas9 (IDT 1081059) was incubated with both sgRNAs for 10 min at 37 °C to form the RNP complex. The GeneWeld pPRISM-5'mitfaHom-nCas9n, gcry1:BFP-3'mitfaHom plasmid was then added to the injection mix along with phenol red (Sigma-Aldrich P0290) . The final concentrations injected into the embryos were: 75 pg/nl Cas9, 12.5 pg/nl *mitfa* sgRNA, 12.5 pg/nl Universal sgRNA, and 5 pg/nl pPRISM plasmid.

Genotyping

Tail clips were taken from 2 month postfertilization (mpf) zebrafish and DNA was extracted using the DNeasy Blood and tissue kit (Qiagen). DNA was PCR amplified with Q5 high fidelity DNA polymerase (NEB). The forward primer MitfaPCR-F binds to the *mitfa* genomic region upstream of the insertion site and the reverse primer 5'homology_amplify-R binds the p2A region of the insertion cassette. Expected PCR amplicon size is 269bp. Amplicons were sequenced using sanger sequencing (Azenta Life Sciences).

RNA-FISH HCR

We adapted the HCR protocol from Ibarra-Garcia-Padilla et al.(*70*). Briefly, embryos were collected and treated with 0.0045% 1-phenyl 2-thiourea (PTU) (Sigma-Aldrich) after 24 hpf to block pigmentation. Embryos were harvested at 72 hpf and fixed in 4% PFA (Santa Cruz) for 24 hrs at 4 °C. Embryos were then washed with PBS and dehydrated/permeabilized with a series of MeOH (Millipore) washes. Embryos were rehydrated with a series of MeOH/PBST washes, permeabilized with acetone (Fisher Scientific) and incubated with Proteinase K (Millipore) for 30 min. This was followed by further fixation with 4% PFA. Embryos were pre-hybridized in probe hybridization buffer (PHB) before incubating them with HCR probes in PHB at concentration of 20nM. Probe sequences for *mitfa* and Cas9 can be found in Supplemental Table 1. Embryos were washed with probe wash buffer before being pre-amplified with probe amplification buffer (PAB). Following pre-amplification, amplifier hairpins were thawed, snap-cooled, and mixed with PAB to a concentration of 36 nM. Embryos were incubated in the hairpin solution followed by washes with 5×SSCT and 1× PBST. Embryos were stained with 2 µg/mL DAPI in PBST and mounted on glass slides. Imaging was performed using a Zeiss LSM880 confocal microscope.

Guide RNA plasmids

The following plasmids were constructed using the Gateway Tol2kit:
zU6A:gRNA-NT;zU6B:gRNA-*ptena*;zU6C:gRNA-*p53*/394,
zU6A:gRNA-NT;zU6B:gRNA-*ptenb*;zU6C:gRNA-*p53*/394,
zU6A:gRNA-*sox10*;zU6B:gRNA-*ptena*;zU6C:gRNA-*p53*/394,
zU6A:gRNA-*sox10*;zU6B:gRNA-*ptenb*;zU6C:gRNA-*p53*/394.

In-fusion cloning (Takara Bio) was used to insert *mitfa:*GFP or *mitfa:*TdTomato into a zU6:gRNA/394 plasmid previously developed in the lab (See Supplementary table 1 for primers used). gRNAs were cloned into zU6:gRNA;*mitfa:*GFP/394 or zU6:gRNA;*mitfa:*TdTomato/394 using BsmBI sites. Other plasmids used in this study that were previously developed in the lab include zU6:gRNA-*ptena*/394, zU6:gRNA-*ptenb*/394, zU6:gRNA-*p53*/394, *mitfa*-BRAF^{V600E};cmlc2:eGFP. All guide RNAs used in this study have previously been validated in zebrafish (*17, 35, 43, 71*).

Transgenic lines

To generate MG-U6:sgRNA stable lines, one-cell-stage embryos from crossing WT and mitfa:Cas9 fish were collected and injected with the 30 pg indicated plasmid and 20 pg tol2 mRNA. Fish with GFP+ melanocytes and BFP+ eyes were selected and outcrossed with WT fish to produce the F1 generation. F1 fish were again sorted and outcrossed to generate F2 generation zebrafish. All fish were imaged on a Zeiss AxioZoom V16 with Zen 2.1 software.

Flow cytometry of melanocytes from adult zebrafish

Zebrafish were euthanized using ice-cold water and dissected using a clean scalpel and forceps. The epidermal and dermal layers of the skin as well as the fins were separated from the rest of the tissues and diced into 1-3mm pieces. Cells were dissociated with Liberase TL (Millipore Sigma 05401020001) and filtered for single cell suspensions as previously described (*43*). Samples were then FACS sorted (BD FACSAria) for GFP+ and GFP- cells. WT fish were used as a GFP negative control. Genomic DNA was isolated from sorted cells using the DNeasy Blood and Tissue Kit (Qiagen).

Tumor Dissection

Fish with tumors were euthanized with ice-cold water and immediately dissected with a scalpel to isolate tumor tissue. Genomic DNA was purified from the tumor samples using the Dneasy Blood and tissue kit (Qiagen).

CRISPR sequencing

Primer pairs were designed to produce amplicons 200 to 280 bp in length with the mutation site within 100 bp from the beginning or end of amplicon (see table S1 for primer sequences). Genomic DNA isolated from methods detailed above was PCR amplified with Q5 high fidelity DNA polymerase (NEB) and run on an agarose gel to visualize PCR products. The samples were then purified using the NucleoSpin Gel and PCR cleanup kit (Takara Bio). Deep sequencing was conducted using the CRISPR-seq platform. Sequencing data was analyzed with CRISPResso2 (*72*) and indel charts were generated with CRISPRVariants R package (*73*).

Drug treatments

Epinephrine hydrochloride (Sigma-Aldrich) was used at 1 mg/ml in fish water. Fish were treated for 10 minutes prior to imaging.

Zebrafish tumor-free survival curves

To generate a transgenic melanoma model, one-cell-stage embryos from WT X mitfa:Cas9 fish crosses were injected with *mitfa*-BRAF^{V600E};cmlc2:eGFP, 20 pg Tol2 mRNA, and the indicated gRNA plasmids for each condition. The total amount of plasmid per embryo did not exceed 30 pg. Embryos were screened for GFP positive hearts and sorted for BFP+ or BFP- eyes. Fish were screened for tumors using a microscope every 2 weeks starting at 4 weeks post fertilization. Tumors were only called if an elevated lesion was observed. Graphpad prism 9 was used to generate and analyze Kaplan-Meier survival curves. Statistical differences were determined using log-rank Mantel–Cox test. All screening and imaging was conducted on a Zeiss AxioZoom V16 using Zen 2.1 software.

Histology

Zebrafish were sacrificed using ice-cold water and placed in 4% paraformaldehyde (Santa Cruz 30525-89-4) in PBS for 72 h at 4°C on a rocker. Fish were then transferred to 70% EtOH for 24 h at 4°C on a rocker. Fish were sent to Histowiz, Inc (Brooklyn, NY, USA), where they were paraffin embedded, sectioned, stained and imaged. All the stainings were performed at Histowiz, Inc Brooklyn, using the Leica Bond RX automated stainer (Leica Microsystems) using a Standard Operating Procedure and fully automated workflow. Samples were processed, embedded in paraffin, and sectioned at 4μm. The slides were dewaxed using xylene and alcohol based dewaxing solutions. Epitope retrieval was performed by heat-induced epitope retrieval (HIER) of the formalin-fixed, paraffin-embedded tissue using Citrate based pH 6 solution (Leica Microsystems, AR9961) for 20 mins at 95 C. The tissues were first incubated with peroxide block buffer (Leica Microsystems), followed by incubation with the following antibodies for 30 min: BRAFV600E antibody (ab228461, 1:100), phospho-AKT antibody (CST4060, 1:50), SOX9 antibody (AB_185230, 1:1000), and SOX10 antibody (GTX128374, 1:500). This was followed by incubation with DAB secondary reagents: polymer, DAB refine and hematoxylin (Bond Polymer Refine Detection Kit, Leica Microsystems) according to the manufacturer's protocol. The slides were dried, coverslipped (TissueTek-Prisma Coverslipper) and visualized using a Leica Aperio AT2 slide scanner (Leica Microsystems) at 40X.

Quantification of SOX10 intensity

FFPE slides were deparaffinized by consecutive incubations in xylene and 100-50% ethanol. For antigen retrieval, slides were placed in 10 mM sodium citrate pH 6.2 in a pressure cooker and heated to 95°C for 20 minutes. Slides were then cooled to room temperature and blocked in 5% donkey serum, 1% BSA, and 0.4% Triton-X100 in PBS for 1 hour at room temperature. The primary antibody targeting SOX10 (GeneTex, GTX128374) was added to the blocking buffer at 1:200 concentration and incubated at 4°C overnight. Slides were then washed in PBS before incubation with the secondary antibody (donkey anti-rabbit Alexa Fluor Plus 488, Thermo Fisher Scientific #AC32790; 1:250) and Hoescht (Thermo Fisher Scientific, #62249; 1:1000) in blocking buffer for 2 hours at room temperature. Slides were mounted in Vectashield Plus (Vector Labs, H-1900). Slides were imaged on a LSM 880 confocal microscope using a 40X oil

immersion objective. 3 images were captured per sample. Quantification of SOX10 intensity per cell was performed using CellProfiler (*74*) and MATLAB r2023b (Mathworks). Cells were segmented in CellProfiler to obtain a nuclear mask from the Hoescht signal and using this mask the mean intensity per nucleus was quantified.

Re-analysis of human melanoma scRNA-seq data

Human melanoma scRNA-seq data from Wouters et al. was accessed from GEO (GSE134432) (*34*). All analysis was done in R (version 4.3.1) using the Seurat package (version 5.0.2)(*75*). Counts matrices for each sample and cell line were imported into R and converted into Seurat objects before merging into one combined Seurat object. Counts were normalized using the Seurat function NormalizeData with default parameters. UMAP was calculated using the Seurat function RunUMAP with 10 dimensions.

Statistical analysis

Statistical significance was analyzed using t test, Log-rank (Mantel-Cox) test, Wilcoxon Rank Sum Test or as indicated in the figure legends. GraphPad Prism 9 software was used for data processing and statistical analysis. *$P < 0.05$; **$P < 0.005$; ***$P < 0.001$; ****$P < 0.0001$. Data are presented as means ± SD unless otherwise indicated.

ACKNOWLEDGEMENTS

We thank members of the White lab for valuable discussions and feedback on this project. We thank Nelly Cruz Esteves for helpful feedback on the manuscript. We also thank the MSKCC flow cytometry core for assistance with cell sorting, Integrated Genomics Operation Core, funded by an NCI Cancer Center Support Grant (P30 CA08748) for sequencing assistance, and Molecular Cytology Core for their help with imaging. We thank the MSKCC aquatics core facility for their support of this work. Schematic figures were all made using Biorender.com with a paid Biorender license.

Funding: RMW was funded through the NIH/NCI Cancer Center Support Grant P30 CA008748, the Melanoma Research Alliance, The Debra and Leon Black Family Foundation, NIH Research Program Grants R01CA229215 and R01CA238317, NIH Director's New Innovator Award DP2CA186572, The Pershing Square Sohn Foundation, The Mark Foundation for Cancer Research, The American Cancer Society, The Alan and Sandra Gerry Metastasis Research Initiative at the Memorial Sloan Kettering Cancer Center, The Harry J. Lloyd Foundation, Consano and the Starr Cancer Consortium. This work was also supported by NIH ORIP R24OD020166 (MM). YM was supported by a Medical Scientist Training Program grant from the NIH under award number T32GM007739 to the Weill Cornell/Rockefeller/Sloan Kettering Tri-Institutional MD-PhD Program and Kirschstein-National Research Service Award (NRSA) predoctoral fellowship under award number F30CA265124. MVH was funded by a K99/R00 Pathway to Independence Award from the National Cancer Institute (1K99CA266931). SP was funded by a Molecular Imaging in Cancer Biology Training Grant at Memorial Sloan Kettering Cancer Center from the National Cancer institute (T32CA254875) and the Ruth L.

Kirschstein National Research Service Award for Individual Predoctoral Fellows from the National Cancer Institute (F31CA271518).

Author contributions:

Conceptualization: SP, RMW
Investigation: SP, YM, MVH, JBS, ZM, JX
Visualization: SP, MVH, JBS
Supervision: TL, MM, RMW
Writing—original draft: SP, RMW
Writing—review & editing: SP, MVH, RMW

Competing interests: MM has competing interests with Recombinetics Inc., LifEngine Technologies, and LifEngine Animal Health Laboratories, Inc. RMW is a paid consultant to N-of-One Therapeutics, a subsidiary of Qiagen and is on the scientific advisory board of Consano but receives no income for this. RMW receives royalty payments for the use of the casper zebrafish line from Carolina Biologicals. SP, YM, MVH, JBS, ZM, JX, and TL declare no competing interests.

Data and materials availability: All data are available in the main text or the supplementary materials, or upon request. Plasmids and other materials generated from this study are available upon request.

REFERENCES

1. L. Solnica-Krezel, A. F. Schier, W. Driever, Efficient recovery of ENU-induced mutations from the zebrafish germline. *Genetics* **136**, 1401-1420 (1994).
2. W. Driever, L. Solnica-Krezel, A. F. Schier, S. C. Neuhauss, J. Malicki, D. L. Stemple, D. Y. Stainier, F. Zwartkruis, S. Abdelilah, Z. Rangini, J. Belak, C. Boggs, A genetic screen for mutations affecting embryogenesis in zebrafish. *Development* **123**, 37-46 (1996).
3. A. Amsterdam, R. M. Nissen, Z. Sun, E. C. Swindell, S. Farrington, N. Hopkins, Identification of 315 genes essential for early zebrafish development. *Proc Natl Acad Sci U S A* **101**, 12792-12797 (2004).
4. E. E. Patton, L. I. Zon, The art and design of genetic screens: zebrafish. *Nat Rev Genet* **2**, 956-966 (2001).
5. J. A. Gagnon, E. Valen, S. B. Thyme, P. Huang, L. Akhmetova, A. Pauli, T. G. Montague, S. Zimmerman, C. Richter, A. F. Schier, Efficient mutagenesis by Cas9 protein-mediated oligonucleotide insertion and large-scale assessment of single-guide RNAs. *PLoS One* **9**, e98186 (2014).
6. G. K. Varshney, W. Pei, M. C. LaFave, J. Idol, L. Xu, V. Gallardo, B. Carrington, K. Bishop, M. Jones, M. Li, U. Harper, S. C. Huang, A. Prakash, W. Chen, R. Sood, J. Ledin, S. M. Burgess, High-throughput gene targeting and phenotyping in zebrafish using CRISPR/Cas9. *Genome Res* **25**, 1030-1042 (2015).
7. H. Kotani, K. Taimatsu, R. Ohga, S. Ota, A. Kawahara, Efficient Multiple Genome Modifications Induced by the crRNAs, tracrRNA and Cas9 Protein Complex in Zebrafish. *PLoS One* **10**, e0128319 (2015).

8. K. A. Dutton, A. Pauliny, S. S. Lopes, S. Elworthy, T. J. Carney, J. Rauch, R. Geisler, P. Haffter, R. N. Kelsh, Zebrafish colourless encodes sox10 and specifies non-ectomesenchymal neural crest fates. *Development* **128**, 4113-4125 (2001).
9. D. M. Parichy, E. M. Mellgren, J. F. Rawls, S. S. Lopes, R. N. Kelsh, S. L. Johnson, Mutational analysis of endothelin receptor b1 (rose) during neural crest and pigment pattern development in the zebrafish Danio rerio. *Dev Biol* **227**, 294-306 (2000).
10. D. S. Eom, L. B. Patterson, R. R. Bostic, D. M. Parichy, Immunoglobulin superfamily receptor Junctional adhesion molecule 3 (Jam3) requirement for melanophore survival and patterning during formation of zebrafish stripes. *Dev Biol* **476**, 314-327 (2021).
11. D. M. Parichy, J. M. Turner, Zebrafish puma mutant decouples pigment pattern and somatic metamorphosis. *Dev Biol* **256**, 242-257 (2003).
12. P. D. Nguyen, G. E. Hollway, C. Sonntag, L. B. Miles, T. E. Hall, S. Berger, K. J. Fernandez, D. B. Gurevich, N. J. Cole, S. Alaei, M. Ramialison, R. L. Sutherland, J. M. Polo, G. J. Lieschke, P. D. Currie, Haematopoietic stem cell induction by somite-derived endothelial cells controlled by meox1. *Nature* **512**, 314-318 (2014).
13. U. Irion, A. P. Singh, C. Nusslein-Volhard, The Developmental Genetics of Vertebrate Color Pattern Formation: Lessons from Zebrafish. *Curr Top Dev Biol* **117**, 141-169 (2016).
14. D. M. Parichy, J. F. Rawls, S. J. Pratt, T. T. Whitfield, S. L. Johnson, Zebrafish sparse corresponds to an orthologue of c-kit and is required for the morphogenesis of a subpopulation of melanocytes, but is not essential for hematopoiesis or primordial germ cell development. *Development* **126**, 3425-3436 (1999).
15. E. E. Patton, H. R. Widlund, J. L. Kutok, K. R. Kopani, J. F. Amatruda, R. D. Murphey, S. Berghmans, E. A. Mayhall, D. Traver, C. D. Fletcher, J. C. Aster, S. R. Granter, A. T. Look, C. Lee, D. E. Fisher, L. I. Zon, BRAF mutations are sufficient to promote nevi formation and cooperate with p53 in the genesis of melanoma. *Curr Biol* **15**, 249-254 (2005).
16. C. J. Ceol, Y. Houvras, J. Jane-Valbuena, S. Bilodeau, D. A. Orlando, V. Battisti, L. Fritsch, W. M. Lin, T. J. Hollmann, F. Ferre, C. Bourque, C. J. Burke, L. Turner, A. Uong, L. A. Johnson, R. Beroukhim, C. H. Mermel, M. Loda, S. Ait-Si-Ali, L. A. Garraway, R. A. Young, L. I. Zon, The histone methyltransferase SETDB1 is recurrently amplified in melanoma and accelerates its onset. *Nature* **471**, 513-517 (2011).
17. C. K. Kaufman, C. Mosimann, Z. P. Fan, S. Yang, A. J. Thomas, J. Ablain, J. L. Tan, R. D. Fogley, E. van Rooijen, E. J. Hagedorn, C. Ciarlo, R. M. White, D. A. Matos, A. C. Puller, C. Santoriello, E. C. Liao, R. A. Young, L. I. Zon, A zebrafish melanoma model reveals emergence of neural crest identity during melanoma initiation. *Science* **351**, aad2197 (2016).
18. W. T. Frantz, C. J. Ceol, From Tank to Treatment: Modeling Melanoma in Zebrafish. *Cells* **9**, (2020).
19. M. S. Ignatius, M. N. Hayes, F. E. Moore, Q. Tang, S. P. Garcia, P. R. Blackburn, K. Baxi, L. Wang, A. Jin, A. Ramakrishnan, S. Reeder, Y. Chen, G. P. Nielsen, E. Y. Chen, R. P. Hasserjian, F. Tirode, S. C. Ekker, D. M. Langenau, tp53 deficiency causes a wide tumor spectrum and increases embryonal rhabdomyosarcoma metastasis in zebrafish. *Elife* **7**, (2018).

20. L. Yin, L. A. Maddison, M. Li, N. Kara, M. C. LaFave, G. K. Varshney, S. M. Burgess, J. G. Patton, W. Chen, Multiplex Conditional Mutagenesis Using Transgenic Expression of Cas9 and sgRNAs. *Genetics* **200**, 431-441 (2015).
21. J. Ablain, E. M. Durand, S. Yang, Y. Zhou, L. I. Zon, A CRISPR/Cas9 vector system for tissue-specific gene disruption in zebrafish. *Dev Cell* **32**, 756-764 (2015).
22. W. Zhou, L. Cao, J. Jeffries, X. Zhu, C. J. Staiger, Q. Deng, Neutrophil-specific knockout demonstrates a role for mitochondria in regulating neutrophil motility in zebrafish. *Dis Model Mech* **11**, (2018).
23. T. T. Ni, J. Lu, M. Zhu, L. A. Maddison, K. L. Boyd, L. Huskey, B. Ju, D. Hesselson, T. P. Zhong, P. S. Page-McCaw, D. Y. Stainier, W. Chen, Conditional control of gene function by an invertible gene trap in zebrafish. *Proc Natl Acad Sci U S A* **109**, 15389-15394 (2012).
24. V. Grajevskaja, D. Camerota, G. Bellipanni, J. Balciuniene, D. Balciunas, Analysis of a conditional gene trap reveals that tbx5a is required for heart regeneration in zebrafish. *PLoS One* **13**, e0197293 (2018).
25. L. Burg, N. Palmer, K. Kikhi, E. S. Miroshnik, H. Rueckert, E. Gaddy, C. MacPherson Cunningham, K. Mattonet, S. L. Lai, R. Marin-Juez, R. B. Waring, D. Y. R. Stainier, D. Balciunas, Conditional mutagenesis by oligonucleotide-mediated integration of loxP sites in zebrafish. *PLoS Genet* **14**, e1007754 (2018).
26. M. Kalvaityte, D. Balciunas, Conditional mutagenesis strategies in zebrafish. *Trends Genet* **38**, 856-868 (2022).
27. R. Singh Angom, Y. Wang, E. Wang, S. K. Dutta, D. Mukhopadhyay, Conditional, Tissue-Specific CRISPR/Cas9 Vector System in Zebrafish Reveals the Role of Nrp1b in Heart Regeneration. *Arterioscler Thromb Vasc Biol* **43**, 1921-1934 (2023).
28. J. Ablain, S. Liu, G. Moriceau, R. S. Lo, L. I. Zon, SPRED1 deletion confers resistance to MAPK inhibition in melanoma. *J Exp Med* **218**, (2021).
29. C. S. Mayer, V. Huser, Learning important common data elements from shared study data: The All of Us program analysis. *PLoS One* **18**, e0283601 (2023).
30. C. Sudlow, J. Gallacher, N. Allen, V. Beral, P. Burton, J. Danesh, P. Downey, P. Elliott, J. Green, M. Landray, B. Liu, P. Matthews, G. Ong, J. Pell, A. Silman, A. Young, T. Sprosen, T. Peakman, R. Collins, UK biobank: an open access resource for identifying the causes of a wide range of complex diseases of middle and old age. *PLoS Med* **12**, e1001779 (2015).
31. A. Tsherniak, F. Vazquez, P. G. Montgomery, B. A. Weir, G. Kryukov, G. S. Cowley, S. Gill, W. F. Harrington, S. Pantel, J. M. Krill-Burger, R. M. Meyers, L. Ali, A. Goodale, Y. Lee, G. Jiang, J. Hsiao, W. F. J. Gerath, S. Howell, E. Merkel, M. Ghandi, L. A. Garraway, D. E. Root, T. R. Golub, J. S. Boehm, W. C. Hahn, Defining a Cancer Dependency Map. *Cell* **170**, 564-576 e516 (2017).
32. K. Kawakami, A. Shima, N. Kawakami, Identification of a functional transposase of the Tol2 element, an Ac-like element from the Japanese medaka fish, and its transposition in the zebrafish germ lineage. *Proc Natl Acad Sci U S A* **97**, 11403-11408 (2000).
33. C. Capparelli, T. J. Purwin, M. Glasheen, S. Caksa, M. Tiago, N. Wilski, D. Pomante, S. Rosenbaum, M. Q. Nguyen, W. Cai, J. Franco-Barraza, R. Zheng, G. Kumar, I. Chervoneva, A. Shimada, V. W. Rebecca, A. E. Snook, K. Hookim, X. Xu, E. Cukierman, M. Herlyn, A. E. Aplin, Targeting SOX10-deficient cells to reduce the dormant-invasive phenotype state in melanoma. *Nat Commun* **13**, 1381 (2022).

34. J. Wouters, Z. Kalender-Atak, L. Minnoye, K. I. Spanier, M. De Waegeneer, C. Bravo Gonzalez-Blas, D. Mauduit, K. Davie, G. Hulselmans, A. Najem, M. Dewaele, D. Pedri, F. Rambow, S. Makhzami, V. Christiaens, F. Ceyssens, G. Ghanem, J. C. Marine, S. Poovathingal, S. Aerts, Robust gene expression programs underlie recurrent cell states and phenotype switching in melanoma. *Nat Cell Biol* **22**, 986-998 (2020).
35. J. M. Welker, W. A. Wierson, M. P. Almeida, C. M. Mann, M. E. Torrie, Z. Ming, S. C. Ekker, K. J. Clark, D. L. Dobbs, J. J. Essner, M. McGrail, GeneWeld: Efficient Targeted Integration Directed by Short Homology in Zebrafish. *Bio Protoc* **11**, e4100 (2021).
36. W. A. Wierson, J. M. Welker, M. P. Almeida, C. M. Mann, D. A. Webster, M. E. Torrie, T. J. Weiss, S. Kambakam, M. K. Vollbrecht, M. Lan, K. C. McKeighan, J. Levey, Z. Ming, A. Wehmeier, C. S. Mikelson, J. A. Haltom, K. M. Kwan, C. B. Chien, D. Balciunas, S. C. Ekker, K. J. Clark, B. R. Webber, B. S. Moriarity, S. L. Solin, D. F. Carlson, D. L. Dobbs, M. McGrail, J. Essner, Efficient targeted integration directed by short homology in zebrafish and mammalian cells. *Elife* **9**, (2020).
37. R. M. White, A. Sessa, C. Burke, T. Bowman, J. LeBlanc, C. Ceol, C. Bourque, M. Dovey, W. Goessling, C. E. Burns, L. I. Zon, Transparent adult zebrafish as a tool for in vivo transplantation analysis. *Cell Stem Cell* **2**, 183-189 (2008).
38. M. Balik-Meisner, L. Truong, E. H. Scholl, R. L. Tanguay, D. M. Reif, Population genetic diversity in zebrafish lines. *Mamm Genome* **29**, 90-100 (2018).
39. J. A. Lister, C. P. Robertson, T. Lepage, S. L. Johnson, D. W. Raible, nacre encodes a zebrafish microphthalmia-related protein that regulates neural-crest-derived pigment cell fate. *Development* **126**, 3757-3767 (1999).
40. L. P. Fernandez, R. L. Milne, G. Pita, J. A. Aviles, P. Lazaro, J. Benitez, G. Ribas, SLC45A2: a novel malignant melanoma-associated gene. *Hum Mutat* **29**, 1161-1167 (2008).
41. W. Branicki, U. Brudnik, J. Draus-Barini, T. Kupiec, A. Wojas-Pelc, Association of the SLC45A2 gene with physiological human hair colour variation. *J Hum Genet* **53**, 966-971 (2008).
42. G. Streisinger, F. Singer, C. Walker, D. Knauber, N. Dower, Segregation analyses and gene-centromere distances in zebrafish. *Genetics* **112**, 311-319 (1986).
43. J. M. Weiss, M. V. Hunter, N. M. Cruz, A. Baggiolini, M. Tagore, Y. Ma, S. Misale, M. Marasco, T. Simon-Vermot, N. R. Campbell, F. Newell, J. S. Wilmott, P. A. Johansson, J. F. Thompson, G. V. Long, J. V. Pearson, G. J. Mann, R. A. Scolyer, N. Waddell, E. D. Montal, T. H. Huang, P. Jonsson, M. T. A. Donoghue, C. C. Harris, B. S. Taylor, T. Xu, R. Chaligne, P. V. Shliaha, R. Hendrickson, A. A. Jungbluth, C. Lezcano, R. Koche, L. Studer, C. E. Ariyan, D. B. Solit, J. D. Wolchok, T. Merghoub, N. Rosen, N. K. Hayward, R. M. White, Anatomic position determines oncogenic specificity in melanoma. *Nature* **604**, 354-361 (2022).
44. L. Hou, H. Arnheiter, W. J. Pavan, Interspecies difference in the regulation of melanocyte development by SOX10 and MITF. *Proc Natl Acad Sci U S A* **103**, 9081-9085 (2006).
45. R. N. Kelsh, M. Brand, Y. J. Jiang, C. P. Heisenberg, S. Lin, P. Haffter, J. Odenthal, M. C. Mullins, F. J. van Eeden, M. Furutani-Seiki, M. Granato, M. Hammerschmidt, D. A. Kane, R. M. Warga, D. Beuchle, L. Vogelsang, C. Nusslein-Volhard, Zebrafish pigmentation mutations and the processes of neural crest development. *Development* **123**, 369-389 (1996).

46. T. J. Carney, K. A. Dutton, E. Greenhill, M. Delfino-Machin, P. Dufourcq, P. Blader, R. N. Kelsh, A direct role for Sox10 in specification of neural crest-derived sensory neurons. *Development* **133**, 4619-4630 (2006).
47. R. L. Cunningham, E. T. Kramer, S. K. DeGeorgia, P. M. Godoy, A. P. Zarov, S. Seneviratne, V. Grigura, C. K. Kaufman, Functional in vivo characterization of sox10 enhancers in neural crest and melanoma development. *Commun Biol* **4**, 695 (2021).
48. J. P. Owen, R. N. Kelsh, C. A. Yates, A quantitative modelling approach to zebrafish pigment pattern formation. *Elife* **9**, (2020).
49. Y. Nagao, H. Takada, M. Miyadai, T. Adachi, R. Seki, Y. Kamei, I. Hara, Y. Taniguchi, K. Naruse, M. Hibi, R. N. Kelsh, H. Hashimoto, Distinct interactions of Sox5 and Sox10 in fate specification of pigment cells in medaka and zebrafish. *PLoS Genet* **14**, e1007260 (2018).
50. M. R. Roh, S. Gupta, K. H. Park, K. Y. Chung, M. Lauss, K. T. Flaherty, G. Jonsson, S. Y. Rha, H. Tsao, Promoter Methylation of PTEN Is a Significant Prognostic Factor in Melanoma Survival. *J Invest Dermatol* **136**, 1002-1011 (2016).
51. G. Palmieri, M. Ombra, M. Colombino, M. Casula, M. Sini, A. Manca, P. Paliogiannis, P. A. Ascierto, A. Cossu, Multiple Molecular Pathways in Melanomagenesis: Characterization of Therapeutic Targets. *Front Oncol* **5**, 183 (2015).
52. S. He, M. W. Zimmerman, H. M. Layden, A. Berezovskaya, J. Etchin, M. W. Martel, G. Thurston, C. B. Jing, E. van Rooijen, C. K. Kaufman, S. J. Rodig, L. I. Zon, E. E. Patton, M. R. Mansour, A. T. Look, Synergistic melanoma cell death mediated by inhibition of both MCL1 and BCL2 in high-risk tumors driven by NF1/PTEN loss. *Oncogene* **40**, 5718-5729 (2021).
53. E. Montal, S. Suresh, Y. Ma, M. M. Tagore, R. M. White, Cancer Modeling by Transgene Electroporation in Adult Zebrafish (TEAZ). *Methods Mol Biol* **2707**, 83-97 (2024).
54. J. A. Croushore, B. Blasiole, R. C. Riddle, C. Thisse, B. Thisse, V. A. Canfield, G. P. Robertson, K. C. Cheng, R. Levenson, Ptena and ptenb genes play distinct roles in zebrafish embryogenesis. *Dev Dyn* **234**, 911-921 (2005).
55. A. Faucherre, G. S. Taylor, J. Overvoorde, J. E. Dixon, J. Hertog, Zebrafish pten genes have overlapping and non-redundant functions in tumorigenesis and embryonic development. *Oncogene* **27**, 1079-1086 (2008).
56. O. Shakhova, P. Cheng, P. J. Mishra, D. Zingg, S. M. Schaefer, J. Debbache, J. Hausel, C. Matter, T. Guo, S. Davis, P. Meltzer, D. Mihic-Probst, H. Moch, M. Wegner, G. Merlino, M. P. Levesque, R. Dummer, R. Santoro, P. Cinelli, L. Sommer, Antagonistic cross-regulation between Sox9 and Sox10 controls an anti-tumorigenic program in melanoma. *PLoS Genet* **11**, e1004877 (2015).
57. K. S. Hoek, O. M. Eichhoff, N. C. Schlegel, U. Dobbeling, N. Kobert, L. Schaerer, S. Hemmi, R. Dummer, In vivo switching of human melanoma cells between proliferative and invasive states. *Cancer Res* **68**, 650-656 (2008).
58. W. L. Russell, E. M. Kelly, P. R. Hunsicker, J. W. Bangham, S. C. Maddux, E. L. Phipps, Specific-locus test shows ethylnitrosourea to be the most potent mutagen in the mouse. *Proc Natl Acad Sci U S A* **76**, 5818-5819 (1979).
59. E. Cerami, J. Gao, U. Dogrusoz, B. E. Gross, S. O. Sumer, B. A. Aksoy, A. Jacobsen, C. J. Byrne, M. L. Heuer, E. Larsson, Y. Antipin, B. Reva, A. P. Goldberg, C. Sander, N.

Schultz, The cBio cancer genomics portal: an open platform for exploring multidimensional cancer genomics data. *Cancer Discov* **2**, 401-404 (2012).

60. L. B. Alexandrov, S. Nik-Zainal, D. C. Wedge, S. A. Aparicio, S. Behjati, A. V. Biankin, G. R. Bignell, N. Bolli, A. Borg, A. L. Borresen-Dale, S. Boyault, B. Burkhardt, A. P. Butler, C. Caldas, H. R. Davies, C. Desmedt, R. Eils, J. E. Eyfjord, J. A. Foekens, M. Greaves, F. Hosoda, B. Hutter, T. Ilicic, S. Imbeaud, M. Imielinski, N. Jager, D. T. Jones, D. Jones, S. Knappskog, M. Kool, S. R. Lakhani, C. Lopez-Otin, S. Martin, N. C. Munshi, H. Nakamura, P. A. Northcott, M. Pajic, E. Papaemmanuil, A. Paradiso, J. V. Pearson, X. S. Puente, K. Raine, M. Ramakrishna, A. L. Richardson, J. Richter, P. Rosenstiel, M. Schlesner, T. N. Schumacher, P. N. Span, J. W. Teague, Y. Totoki, A. N. Tutt, R. Valdes-Mas, M. M. van Buuren, L. van 't Veer, A. Vincent-Salomon, N. Waddell, L. R. Yates, I. Australian Pancreatic Cancer Genome, I. B. C. Consortium, I. M.-S. Consortium, I. PedBrain, J. Zucman-Rossi, P. A. Futreal, U. McDermott, P. Lichter, M. Meyerson, S. M. Grimmond, R. Siebert, E. Campo, T. Shibata, S. M. Pfister, P. J. Campbell, M. R. Stratton, Signatures of mutational processes in human cancer. *Nature* **500**, 415-421 (2013).
61. P. F. Cheng, O. Shakhova, D. S. Widmer, O. M. Eichhoff, D. Zingg, S. C. Frommel, B. Belloni, M. I. Raaijmakers, S. M. Goldinger, R. Santoro, S. Hemmi, L. Sommer, R. Dummer, M. P. Levesque, Methylation-dependent SOX9 expression mediates invasion in human melanoma cells and is a negative prognostic factor in advanced melanoma. *Genome Biol* **16**, 42 (2015).
62. X. Yang, R. Liang, C. Liu, J. A. Liu, M. P. L. Cheung, X. Liu, O. Y. Man, X. Y. Guan, H. L. Lung, M. Cheung, SOX9 is a dose-dependent metastatic fate determinant in melanoma. *J Exp Clin Cancer Res* **38**, 17 (2019).
63. S. M. Hossain, M. R. Eccles, Phenotype Switching and the Melanoma Microenvironment; Impact on Immunotherapy and Drug Resistance. *Int J Mol Sci* **24**, (2023).
64. J. Travnickova, S. Wojciechowska, A. Khamseh, P. Gautier, D. V. Brown, T. Lefevre, A. Brombin, A. Ewing, A. Capper, M. Spitzer, R. Dilshat, C. A. Semple, M. E. Mathers, J. A. Lister, E. Steingrimsson, T. Voet, C. P. Ponting, E. E. Patton, Zebrafish MITF-Low Melanoma Subtype Models Reveal Transcriptional Subclusters and MITF-Independent Residual Disease. *Cancer Res* **79**, 5769-5784 (2019).
65. N. Sun, S. Petiwala, R. Wang, C. Lu, M. Hu, S. Ghosh, Y. Hao, C. P. Miller, N. Chung, Development of drug-inducible CRISPR-Cas9 systems for large-scale functional screening. *BMC Genomics* **20**, 225 (2019).
66. Y. Huang, B. Q. Gao, Q. Meng, L. Z. Yang, X. K. Ma, H. Wu, Y. H. Pan, L. Yang, D. Li, L. L. Chen, CRISPR-dCas13-tracing reveals transcriptional memory and limited mRNA export in developing zebrafish embryos. *Genome Biol* **24**, 15 (2023).
67. G. Kushawah, L. Hernandez-Huertas, J. Abugattas-Nunez Del Prado, J. R. Martinez-Morales, M. L. DeVore, H. Hassan, I. Moreno-Sanchez, L. Tomas-Gallardo, A. Diaz-Moscoso, D. E. Monges, J. R. Guelfo, W. C. Theune, E. O. Brannan, W. Wang, T. J. Corbin, A. M. Moran, A. Sanchez Alvarado, E. Malaga-Trillo, C. M. Takacs, A. A. Bazzini, M. A. Moreno-Mateos, CRISPR-Cas13d Induces Efficient mRNA Knockdown in Animal Embryos. *Dev Cell* **54**, 805-817 e807 (2020).

68. J. M. Weiss, D. Lumaquin-Yin, E. Montal, S. Suresh, C. S. Leonhardt, R. M. White, Shifting the focus of zebrafish toward a model of the tumor microenvironment. *Elife* **11**, (2022).
69. L. E. Jao, S. R. Wente, W. Chen, Efficient multiplex biallelic zebrafish genome editing using a CRISPR nuclease system. *Proc Natl Acad Sci U S A* **110**, 13904-13909 (2013).
70. R. Ibarra-Garcia-Padilla, A. G. A. t. Howard, E. W. Singleton, R. A. Uribe, A protocol for whole-mount immuno-coupled hybridization chain reaction (WICHCR) in zebrafish embryos and larvae. *STAR Protoc* **2**, 100709 (2021).
71. S. Suresh, R. Rabbie, M. Garg, D. Lumaquin, T. H. Huang, E. Montal, Y. Ma, N. M. Cruz, X. Tang, J. Nsengimana, J. Newton-Bishop, M. V. Hunter, Y. Zhu, K. Chen, E. de Stanchina, D. J. Adams, R. M. White, Identifying the Transcriptional Drivers of Metastasis Embedded within Localized Melanoma. *Cancer Discov* **13**, 194-215 (2023).
72. K. Clement, H. Rees, M. C. Canver, J. M. Gehrke, R. Farouni, J. Y. Hsu, M. A. Cole, D. R. Liu, J. K. Joung, D. E. Bauer, L. Pinello, CRISPResso2 provides accurate and rapid genome editing sequence analysis. *Nat Biotechnol* **37**, 224-226 (2019).
73. H. Lindsay, A. Burger, B. Biyong, A. Felker, C. Hess, J. Zaugg, E. Chiavacci, C. Anders, M. Jinek, C. Mosimann, M. D. Robinson, CrispRVariants charts the mutation spectrum of genome engineering experiments. *Nat Biotechnol* **34**, 701-702 (2016).
74. D. R. Stirling, M. J. Swain-Bowden, A. M. Lucas, A. E. Carpenter, B. A. Cimini, A. Goodman, CellProfiler 4: improvements in speed, utility and usability. *BMC Bioinformatics* **22**, 433 (2021).
75. Y. Hao, T. Stuart, M. H. Kowalski, S. Choudhary, P. Hoffman, A. Hartman, A. Srivastava, G. Molla, S. Madad, C. Fernandez-Granda, R. Satija, Dictionary learning for integrative, multimodal and scalable single-cell analysis. *Nat Biotechnol* **42**, 293-304 (2024).

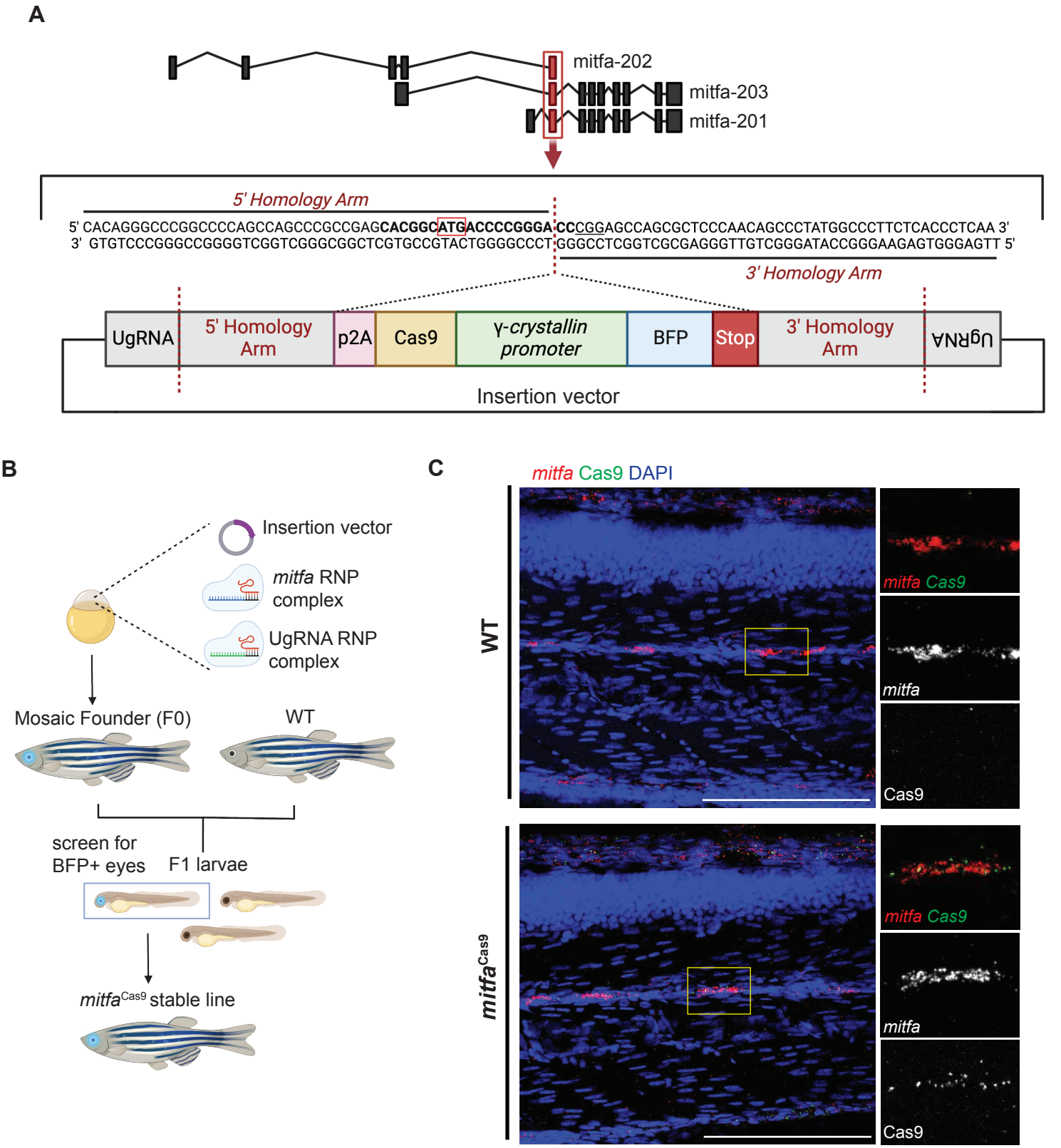
A
mitfa-202
mitfa-203
mitfa-201
5' Homology Arm
5' CACAGGGCCCGGCCCCAGCCAGCCCGCCGAGCACGGCATGACCCCGGGACCCGGAGCCAGCGCTCCCAACAGCCCTATGGCCCTTCTCACCCTCAA 3'
3' GTGTCCCGGGCCGGGGTCGGTCGGGCGGCTCGTGCCGTACTGGGGCCCTGGGCCTCGGTCGCGAGGGTTGTCGGGATACCGGGAAGAGTGGGAGTT 5'
3' Homology Arm
UgRNA
5' Homology Arm
p2A
Cas9
γ-crystallin promoter
BFP
Stop
3' Homology Arm
UgRNA
Insertion vector
B
Insertion vector
mitfa RNP complex
UgRNA RNP complex
Mosaic Founder (F0)
WT
screen for BFP+ eyes
F1 larvae
mitfaCas9 stable line
C
mitfa Cas9 DAPI
WT
mitfa Cas9
mitfa
Cas9
mitfaCas9
mitfa Cas9
mitfa
Cas9

Fig. 1. Targeted integration of Cas9 to the *mitfa* locus with GeneWeld KI system.
(A) Schematic depicting integration site and GeneWeld knock-in cassette. 5' and 3' homology arms are designed to target exon 2 of the zebrafish *mitfa* gene. The knock-in cassette includes p2A followed by Cas9 and BFP driven by the eye-specific promoter gamma-crystallin. **(B)** Pipeline to produce F1 mitfa^{Cas9} zebrafish. The GeneWeld knock-in vector and gRNAs targeting the *mitfa* genomic insertion site or specific sites on the knock-in vector (UgRNA) are co-injected into one-cell stage wild-type zebrafish embryos. Embryos are screened for BFP+ eyes marking mosaic integration. These mosaic founder fish are then raised to adulthood and crossed with wild-type fish. The resulting embryos are screened for BFP+ eyes and sequenced to confirm precise integration. **(C)** Fluorescent in situ hybridization chain reaction (FISH) on 3dpf wild-type and *mitfa*^{Cas9} embryos treated with 1-phenyl 2-thiourea (PTU). The presence of *mitfa* and Cas9 RNA was assessed by confocal microscopy at 40x magnification. Maximum intensity projections are shown. n=17 WT embryos and n=16 mitfa^{Cas9} embryos were screened. Scale bars, 100µm.

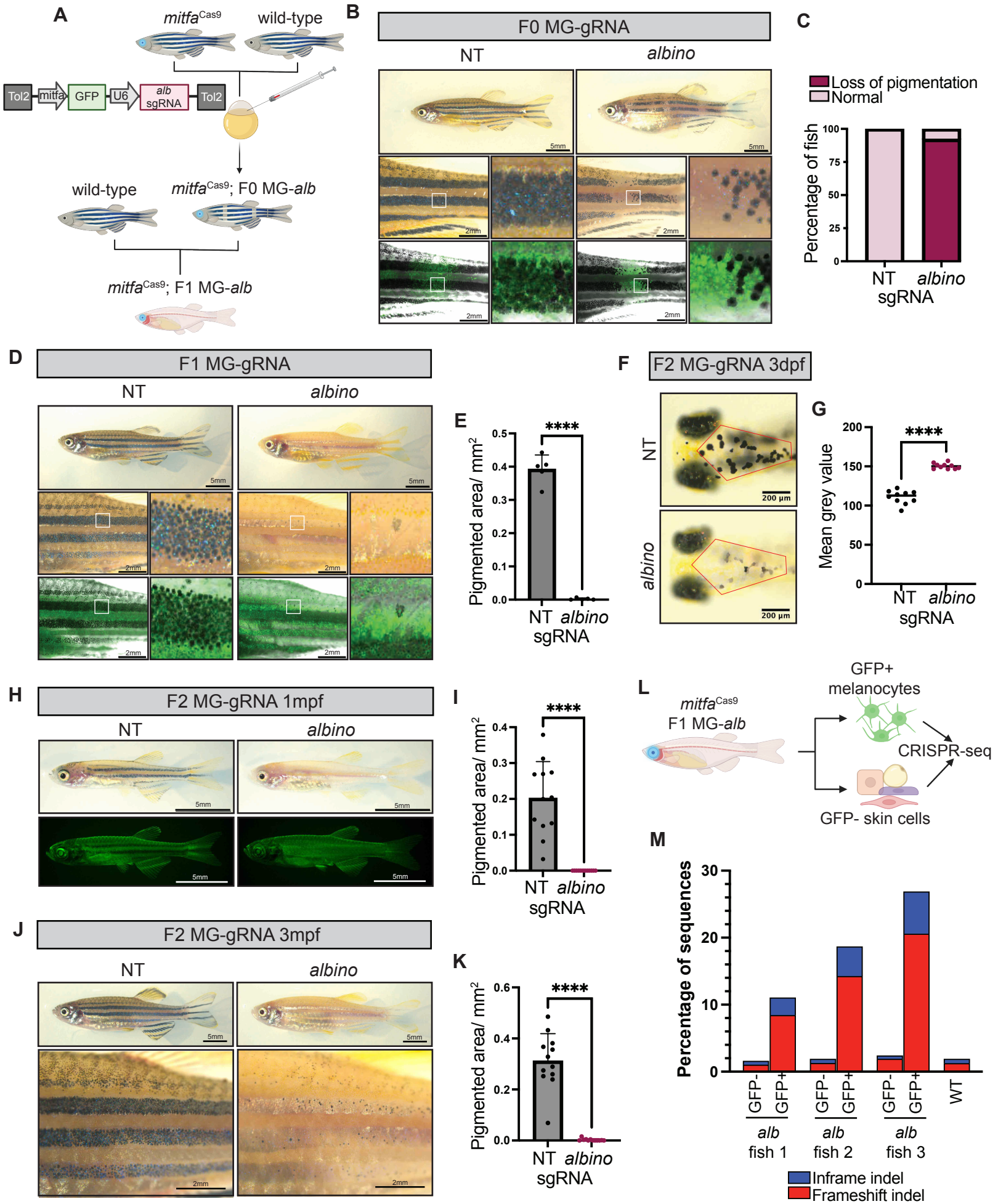
A
mitfa^Cas9
wild-type
Tol2
mitfa
GFP
U6
alb sgRNA
Tol2
wild-type
mitfa^Cas9; F0 MG-alb
mitfa^Cas9; F1 MG-alb
B
F0 MG-gRNA
NT
albino
C
Loss of pigmentation
Normal
Percentage of fish
NT
albino
sgRNA
D
F1 MG-gRNA
NT
albino
E
Pigmented area/ mm²
****
NT
albino
sgRNA
F
F2 MG-gRNA 3dpf
NT
albino
200 µm
G
Mean grey value
****
NT
albino
sgRNA
H
F2 MG-gRNA 1mpf
NT
albino
I
Pigmented area/ mm²
****
NT
albino
sgRNA
L
mitfa^Cas9
F1 MG-alb
GFP+ melanocytes
CRISPR-seq
GFP- skin cells
J
F2 MG-gRNA 3mpf
NT
albino
K
Pigmented area/ mm²
****
NT
albino
sgRNA
M
Percentage of sequences
GFP-
GFP+
alb fish 1
alb fish 2
alb fish 3
WT
Inframe indel
Frameshift indel

Fig. 2. Melanocyte lineage-specific knockout of *albino* using *mitfa*^{Cas9} fish.
(A) Pipeline to generate F0 and F1 *mitfa*:GFP;U6:gRNA (MG-gRNA) zebrafish. **(B)** Adult mitfa^{Cas9} MG-NT and MG-*albino* F0 fish. **(C)** Proportion of MG-NT (n=11) and MG-*albino* (n=12) F0 fish with loss of pigmentation phenotype. **(D)** Adult mitfa^{Cas9} MG-NT and MG-*albino* F1 fish. **(E)** Pigmented area/ mm^2 calculated for n=5 fish/ genotype within a defined rectangular region of interest (ROI) encompassing the top and middle melanocyte stripes. Two-sided student's *t*-test was used to assess statistical significance, **** $p < 0.0001$; error bars, SD. **(F)** 3dpf mitfa^{Cas9} MG-NT and MG-*albino* F2 fish. Three representative embryos are shown for each genotype. **(G)** Mean grey value of head melanocytes calculated for n=10 embryos/genotype within a defined hexagonal ROI indicated as a red outline in 2F. Two-sided student's *t*-test was used to assess statistical significance, **** $p < 0.0001$. **(H)** 1mpf mitfa^{Cas9} MG-NT and MG-*albino* F2 fish. Three representative fish are shown for each genotype. **(I)** Pigmented area/ mm^2 calculated for n=12 fish/ genotype within a defined rectangular region of interest (ROI) encompassing the top and middle melanocyte stripes. Two-sided student's *t*-test was used to assess statistical significance, **** $p < 0.0001$; error bars, SD. **(J)** 3mpf mitfa^{Cas9} MG-NT and MG-*albino* F2 fish. Three representative fish are shown for each genotype. **(K)** Pigmented area/ mm^2 calculated for n=12 fish/ genotype within a defined rectangular region of interest (ROI) encompassing the top and middle melanocyte stripes. Two-sided student's *t*-test was used to assess statistical significance, **** $p < 0.0001$; error bars, SD. **(L)** Schematic for CRISPR sequencing protocol. **(M)** CRISPR-seq results are shown for WT and n=3 independent F1 MG-*albino* fish. Only GFP- cells were isolated from WT fish. Results are shown as a fraction of sequences with indels calculated using CRISPRESSO.

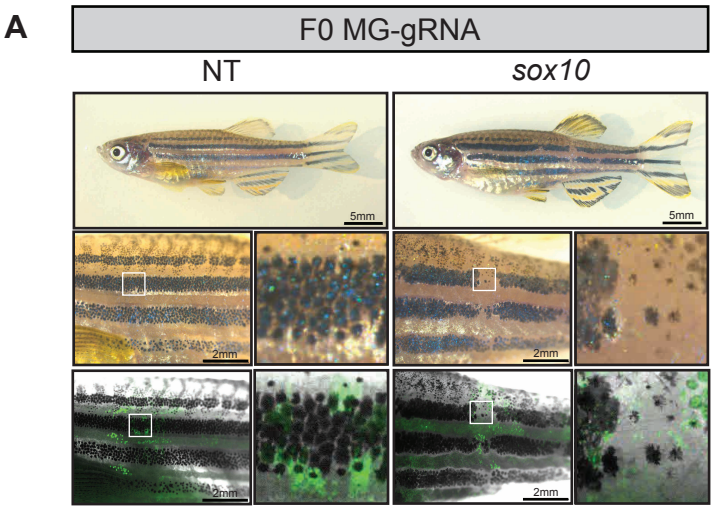
A
F0 MG-gRNA
NT
sox10
5mm
2mm

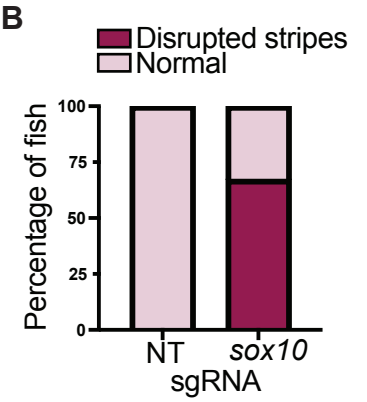
B
Disrupted stripes
Normal
Percentage of fish
100
75
50
25
0
NT
sox10
sgRNA

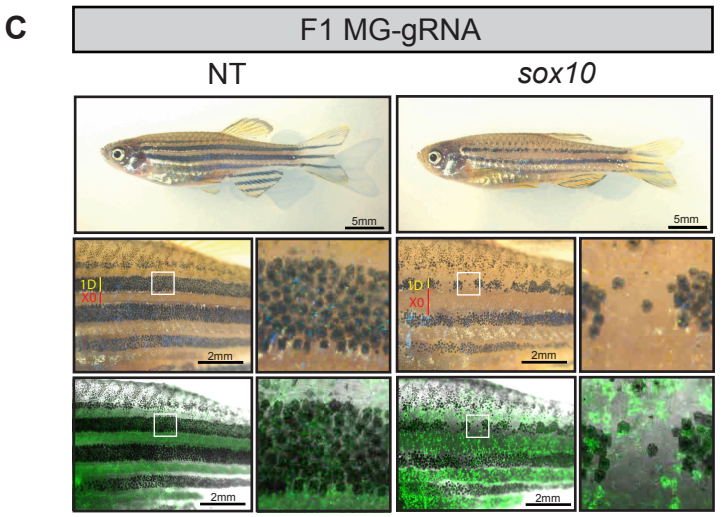
C
F1 MG-gRNA
NT
sox10
5mm
1D
X0
2mm

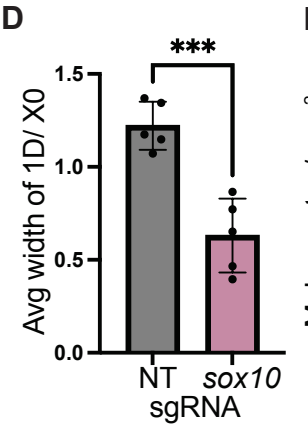
D
***
Avg width of 1D/ X0
1.5
1.0
0.5
0.0
NT
sox10
sgRNA

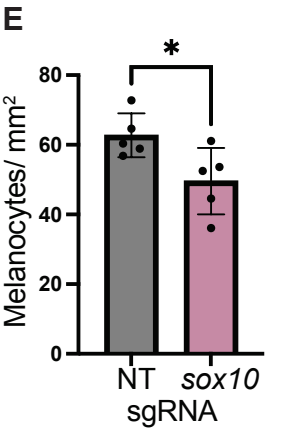
E
*
Melanocytes/ mm2
80
60
40
20
0
NT
sox10
sgRNA

Fig. 3. Melanocyte lineage-specific knockout of *sox10* using *mitfa*^{Cas9} fish.
(A) Adult mitfa^{Cas9} MG-NT and MG-*sox10* F0 fish. **(B)** Proportion of MG-NT (n=11) and MG-*sox10* (n=6) F0 fish with disrupted stripes phenotype. **(C)** Adult mitfa^{Cas9} MG-NT and MG-*sox10* F1 fish. **(D)** The average width of melanocyte stripe 1D and xanthophore interstripe X0 was calculated for each fish by averaging 5 stripe/interstripe width measurements. N=5 fish per genotype. Two-sided student's *t*-test was used to assess statistical significance, *** $p < 0.001$; error bars, SD. **(E)** F1 MG-NT (n=5) and MG-*sox10* (n=5) adult fish were treated with epinephrine and melanocytes were counted within a defined rectangular region of interest 3.46mm x 2.54mm encompassing the top and middle melanocyte stripes. Two-sided student's *t*-test was used to assess statistical significance, * $p < 0.05$; error bars, SD.

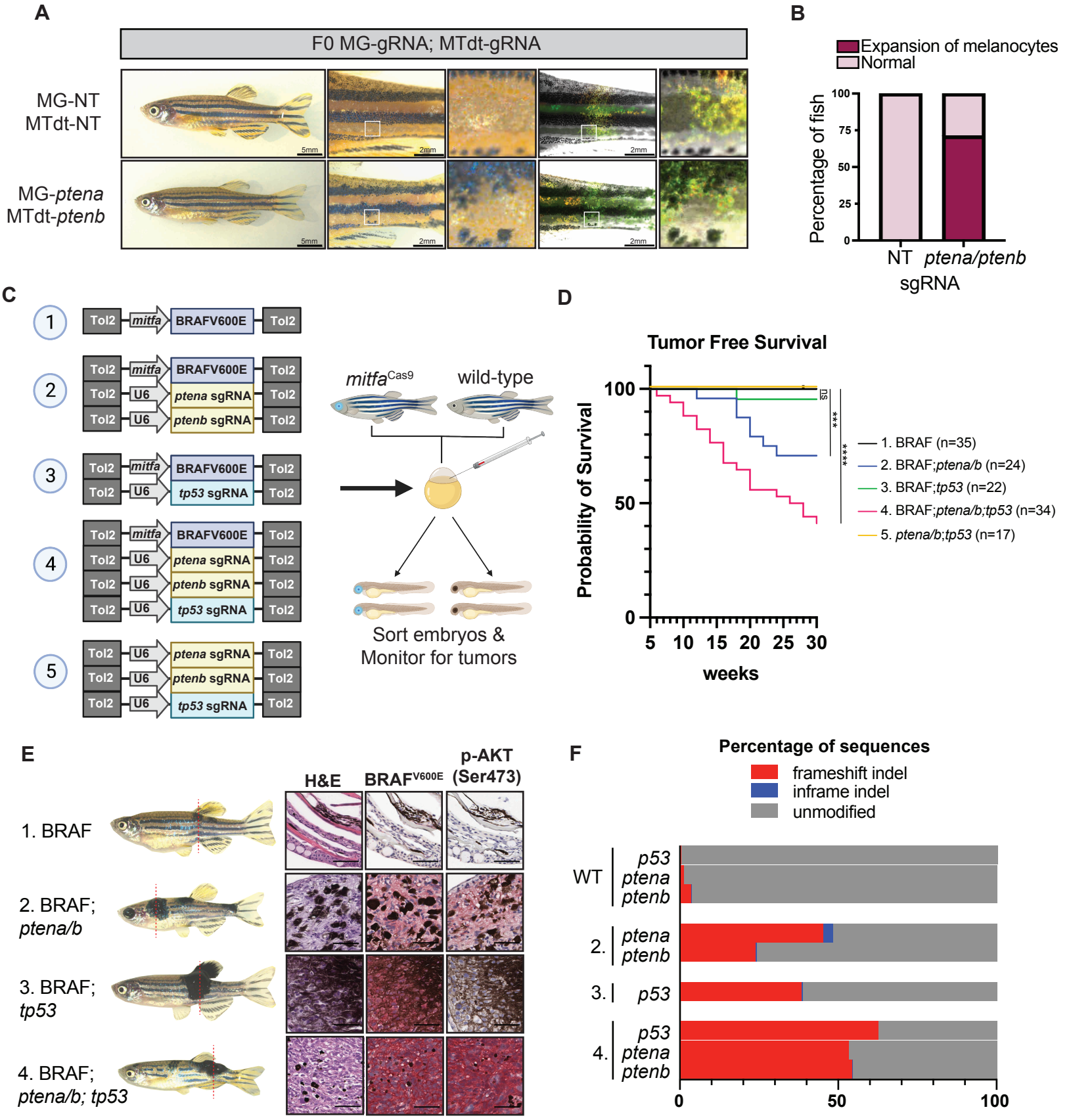
A
F0 MG-gRNA; MTdt-gRNA
MG-NT
MTdt-NT
MG-ptena
MTdt-ptenb
5mm
2mm
B
Expansion of melanocytes
Normal
Percentage of fish
100
75
50
25
0
NT
ptena/ptenb
sgRNA
C
1
Tol2
mitfa
BRAFV600E
2
U6
ptena sgRNA
ptenb sgRNA
3
tp53 sgRNA
4
5
mitfaCas9
wild-type
Sort embryos &
Monitor for tumors
D
Tumor Free Survival
Probability of Survival
weeks
5
10
15
20
25
30
ns
***
****
1. BRAF (n=35)
2. BRAF;ptena/b (n=24)
3. BRAF;tp53 (n=22)
4. BRAF;ptena/b;tp53 (n=34)
5. ptena/b;tp53 (n=17)
E
H&E
BRAFV600E
p-AKT
(Ser473)
1. BRAF
2. BRAF;
ptena/b
3. BRAF;
tp53
4. BRAF;
ptena/b; tp53
F
Percentage of sequences
frameshift indel
inframe indel
unmodified
WT
p53
ptena
ptenb
2.
3.
4.
0
50
100

Fig. 4. Generation of a zebrafish melanoma model in *mitfa*^{Cas9} fish.
(A) Adult mitfa^{Cas9} MG-NT; *mitfa*:TdT;U6:NT (MTdt-NT) and MG-*ptena*; MTdT-*ptenb* F0 fish. **(B)** Proportion of MG-NT; MTdT-NT (n=6) and MG-*ptena*; MTdT-*ptenb* (n=7) F0 fish with disrupted stripes phenotype. **(C)** Schematic of zebrafish tumorigenesis assay. Indicated plasmids are injected into one-cell stage embryos from crosses between mitfa^{Cas9} and WT fish. The mitfa:BRAF^{V600E} plasmid includes cardiac-specific cmlc2:GFP. Embryos were sorted for GFP+ hearts and BFP+ eyes and fish were screened every 2 weeks for tumors. **(D)** Tumor free survival curve. N=2 independent experiments. Tumors were tracked over the course of 30 weeks. Log-rank (Mantel-Cox) test was used to assess statistical significance, *** $p < 0.001$; **** $p < 0.0001$; ns: no significance. **(E)** Histology was performed on one fish from each indicated injection group. Dotted lines indicate site of sectioning. Red chromogen was used for all IHC staining. Scale bars, 50µm. **(F)** CRISPR-seq results are shown for normal skin dissected from WT fish and tumors dissected from injection conditions 2, 3, and 4. Results are shown as a fraction of sequences with indels calculated using CRISPRESSO.

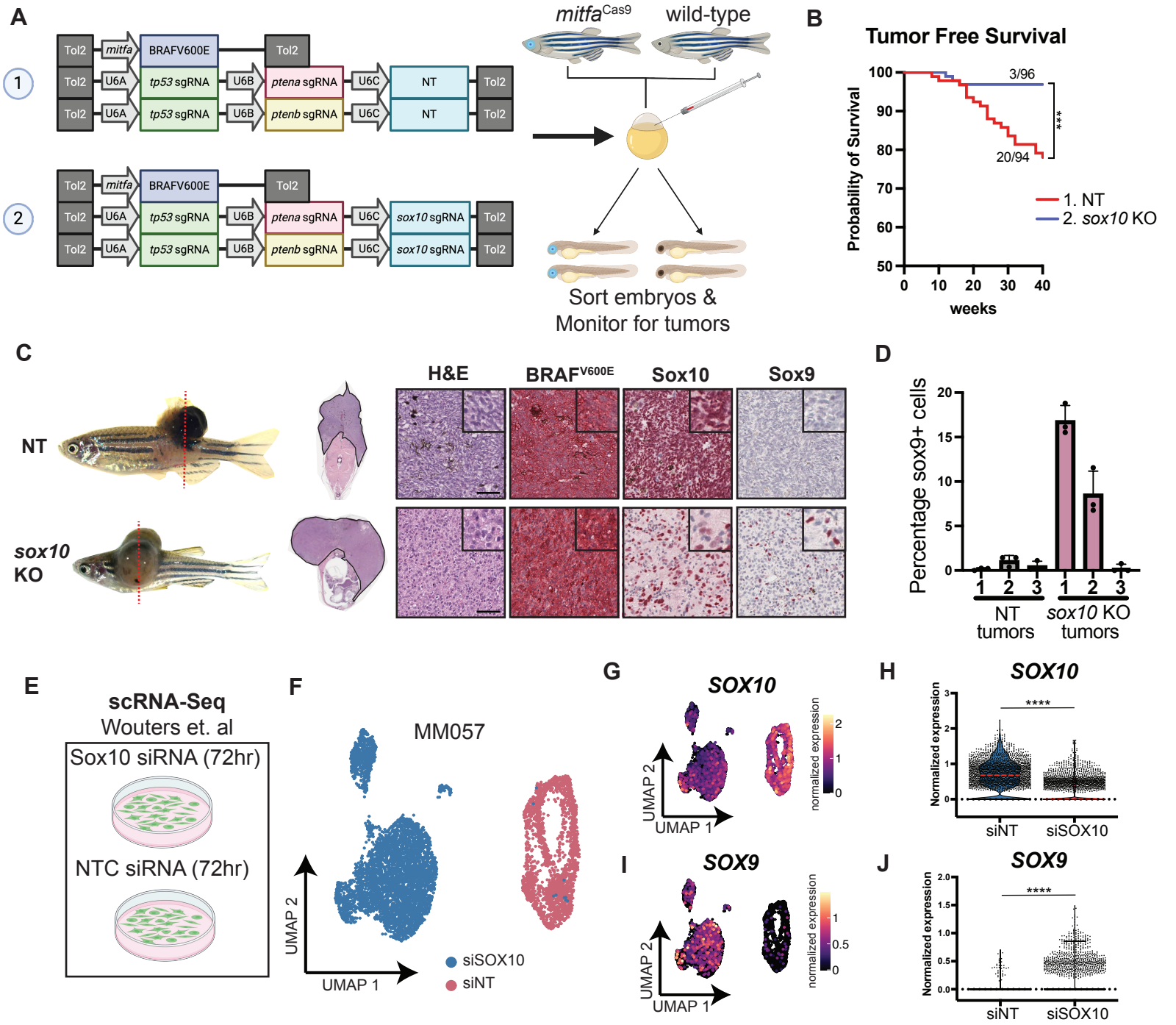
A
1
Tol2
mitfa
BRAFV600E
Tol2
U6A
tp53 sgRNA
U6B
ptena sgRNA
U6C
NT
Tol2
U6A
tp53 sgRNA
U6B
ptenb sgRNA
U6C
NT
Tol2
2
Tol2
mitfa
BRAFV600E
Tol2
U6A
tp53 sgRNA
U6B
ptena sgRNA
U6C
sox10 sgRNA
Tol2
U6A
tp53 sgRNA
U6B
ptenb sgRNA
U6C
sox10 sgRNA
Tol2
mitfaCas9
wild-type
Sort embryos &
Monitor for tumors
B
Tumor Free Survival
Probability of Survival
100
90
80
70
60
50
0
10
20
30
40
weeks
3/96
20/94
***
1. NT
2. sox10 KO
C
NT
sox10
KO
H&E
BRAFV600E
Sox10
Sox9
D
Percentage sox9+ cells
20
15
10
5
0
1
2
3
1
2
3
NT
tumors
sox10 KO
tumors
E
scRNA-Seq
Wouters et. al
Sox10 siRNA (72hr)
NTC siRNA (72hr)
F
MM057
UMAP 2
UMAP 1
siSOX10
siNT
G
SOX10
UMAP 2
UMAP 1
normalized expression
2
1
0
H
SOX10
Normalized expression
3
2
1
0
****
siNT
siSOX10
I
SOX9
UMAP 2
UMAP 1
normalized expression
1
0.5
0
J
SOX9
Normalized expression
2.0
1.5
1.0
0.5
0.0
****
siNT
siSOX10

Fig. 5. Melanoma specific knockout of *sox10* reduces tumor burden and induces phenotypic switching.

(A) Schematic of zebrafish tumorigenesis assay. Indicated plasmids are injected into one-cell stage embryos from crosses between mitfa^{Cas9} and WT fish. Embryos were sorted for GFP+ hearts and BFP+ eyes and fish were screened every 2 weeks for tumors. **(B)** Tumor free survival curve. N=3 independent experiments. Tumors were tracked over the course of 40 weeks. Log-rank (Mantel-Cox) test was used to assess statistical significance, *** $p < 0.001$. **(C)** Histology is shown for one fish from each injection group. Dotted lines indicate site of sectioning. Red chromogen was used for all IHC staining. Scale bars, 50µm. **(D)** Color thresholding was used on IHC images to calculate the percentage of nuclei that stained positive for *sox9*. NT-1 n=1222 cells, NT-2 n=1620 cells, NT-3 n=2185 cells, sox10-1 n=970 cells, sox10-2 n=594, sox10-3 n=1046. Cells from n=3 images were analyzed for each tumor. **(E)** Schematic of scRNA-seq experimental setup from Wouters et al. Patient derived cell lines were treated with siRNAs targeting SOX10 or NTC and scRNA-seq was conducted at 72hrs. **(F)** UMAP of scRNA-seq dataset for MM057 cell line from Wouters et al. Cells from siSOX10 and siNT conditions are labeled. **(G)** Normalized expression of SOX10 per cell in UMAP space. **(H)** Violin plots of normalized expression of SOX10 per cell. Median is shown as dashed red line. Wilcoxon Rank Sum Test was used to assess statistical significance, **** $p < 0.0001$. **(I)** Normalized expression of SOX9 per cell in UMAP space. **(J)** Violin plots of normalized expression of SOX9 per cell. Wilcoxon Rank Sum Test was used to assess statistical significance, **** $p < 0.0001$.